Nonequilibrium transport in the Anderson model of a biased quantum dot: Scattering Bethe ansatz phenomenology

Sung-Po Chao[1] and Guillaume Palacios[1,2]

[1]*Center for Materials Theory, Department of Physics and Astronomy, Rutgers University, Piscataway, New Jersey 08854, USA*

[2]*Instituut voor Theoretische Fysica, Universiteit van Amsterdam, Valckenierstraat 65, NL-1018 XE Amsterdam, The Netherlands*

(Received 13 April 2010; revised manuscript received 17 January 2011; published 11 May 2011)

We derive the transport properties of a quantum dot subject to a source-drain bias voltage at zero temperature and magnetic field. Using the scattering Bethe anstaz, a generalization of the traditional thermodynamic Bethe ansatz to open systems out of equilibrium, we derive results for the quantum dot occupation in and out of equilibrium and, by introducing *phenomenological* spin- and charge-fluctuation distribution functions in the computation of the current, obtain the differential conductance for large $\frac{U}{\Gamma}$. The Hamiltonian to describe the quantum dot system is the Anderson impurity Hamiltonian and the current and dot occupation as a function of voltage are obtained numerically. We also vary the gate voltage and study the transition from the mixed valence to the Kondo regime in the presence of a nonequilibrium current. We conclude with the difficulty we encounter in this model and a possible way to solve it without resorting to a *phenomenological* method.

DOI: 10.1103/PhysRevB.83.195314 PACS number(s): 72.15.Qm, 72.10.Bg, 72.10.Fk

I. INTRODUCTION

The past few years have witnessed a spectacular progress in the fabrication and exploration of nanostructures giving experimentalists unprecedented control over the microscopic parameters governing the physics of these systems. Nanostructures, beyond their practical applications, display an array of emergent phenomena stemming from their reduced dimensionality which enhances quantum fluctuations and strong correlations. Often, experiments are carried out under nonequilibrium conditions, with currents passing through the structures. The measurements are performed over a wide range of parameters, such as temperature and applied bias, allowing experimental exploration of the interplay between nonequilibrium dynamics and strong correlation physics.[1–6] A canonical example is the nonequilibrium Kondo effect observed in a quantum dot attached to two leads held at different chemical potentials μ_i. The voltage difference $V = \mu_1 - \mu_2$ induces a nonequilibrium current $I(V)$ through the dot, interfering with and eventually destroying the Kondo effect as the voltage is increased.

The standard theoretical description of the transport trough a quantum dot is the two-lead Anderson impurity model under a bias voltage. The one- or two-lead Hamiltonian at zero bias is exactly solvable via Bethe ansatz.[7,8] Using this exact solution as well as NRG calculations, for example, the thermodynamics of the model have been studied in great detail. However, the nonequilibrium situation, namely, when the two leads experience each a different chemical potential, is much more difficult. This is due to the subtle interplay between the nonequilibrium aspect of the problem on one hand and the presence of strong interactions on the other hand. Technically speaking, it is a very nontrivial task to find a basis of states that diagonalize simultaneously the voltage term and the interaction term in the Hamiltonian. Nevertheless, a lot of efforts have been put forward to study this model, but so far only approximate ways of dealing with the voltage and/or the interactions have been developed.[9–24]

In this paper we develop a *phenomenological* approach to the problem, based on the scattering Bethe ansatz (SBA), recently developed by P. Mehta and N. Andrei (MA),[25] a nonperturbative implementation of the Keldysh formalism to construct the current-carrying, *open-system* scattering eigenstates for the two-lead nonequilibrium Anderson impurity mode. The basic idea of the SBA is to construct scattering eigenstates of the full Hamiltonian defined directly on the infinite line and match the incoming states by two Fermi seas describing the initial states of the leads. The nonequilibrium steady-state transport properties of the system are then expressed as expectation values of the current or dot occupation operators in these eigenstates. This program has been implemented for the interacting resonance level model (IRLM), a spinless interacting model, described in Ref. 25 where the zero-temperature results for current and dot occupation $\langle \hat{n}_d \rangle$ for all bias voltages were presented. Another exact solution of this model at the so-called self-dual point[26] by E. Boulat, H. Saleur, and P. Schmitteckert in Refs. 27 and 28 uses conformal field theory techniques and compares successfully with time-dependent density-matrix renormalization group results.

The main motivation of the present paper is to test the very interesting ideas behind the SBA framework on a physically more relevant model such as the Anderson impurity model and to focus on the phenomenology that can be extracted from it. Carrying out the program for the nonequilibrium Anderson model we find difficulties in the direct application of the SBA approach due to the fact that the ground state in the Bethe basis consists of bound pairs of quasiparticles, leading to problems in the computation of the scattering phase shifts for the quasiparticles with complex momenta. This problem is not present in the IRLM when the Bethe momenta are below the impurity level and no bound states can be formed. We circumvent this difficulty by means of the following argument: The transport property computed in the IRLM is related to the single-particle phase shift across the impurity in the Bethe basis. Based on the same idea we develop a phenomenological approach to describe the transport property in the Anderson impurity model. We identify two types of possible phase shifts across impurity, which we refer

to as "spin-fluctuation" and "charge-fluctuation" types to label two phenomenological phase shifts akin to the fundamental excitations described in the traditional Bethe ansatz in this model. The phenomenological ansatz is checked against exact results on the dot occupation in equilibrium and the Friedel sum rule,[29,30] in the linear response regime. Subsequently, we discuss our results for the out-of-equilibrium current, conductance, and dot occupation. The scaling relations for the conductance, predicted from the Fermi liquid picture of the problem at strong and weak coupling, are also discussed.

The paper is organized as follows. We start with a formal construction of scattering eigenstates in the two-lead Anderson impurity model. Then we discuss how we impose boundary conditions, which serve as initial condition in the time-dependent picture, on the electrons within the leads. Next we discuss our results for the dot occupation in equilibrium and the conductance in the linear response regime. Based on the checks in equilibrium we then extend our computation to the out-of-equilibrium regime. The difficulty we encounter for complex momenta and the way we handle it is also addressed there. Comparison with another attempt of exact solution for this model by R. M. Konik *et al.*[31,32] with the idea of dressed excitations above Fermi energy in the Bethe ansatz picture, first considered for the exact conductance of point contact device in the FQHE regime,[33,34] is discussed. We also comment on the validity and implication of our numerical results, among them the charge susceptibility, in the out-of-equilibrium regime. Qualitative agreement between our theory and experimental result is then presented. The limit of $U \to \infty$ is also summarized in the last section based on the same phenomenological approach. Finally, we summarize our results and conclude with some issues on the SBA approach to this model and state how they could be overcome.

II. THE SCATTERING BETHE ANSATZ APPROACH

A. Scattering-state construction

In this section we apply the SBA approach to construct the scattering states of the full Hamiltonian. The (unfolded) two-lead Anderson impurity Hamiltonian reads

$$\hat{H} = \sum_{i=1,2} \int dx\, \psi^\dagger_{i\sigma}(x)(-i\partial_x)\psi_{i\sigma}(x) + \epsilon_d d^\dagger_\sigma d_\sigma + t_i[\psi^\dagger_{i\sigma}(0)\, d_\sigma + d^\dagger_\sigma \psi_{i\sigma}(0)] + U\, d^\dagger_\uparrow d_\uparrow d^\dagger_\downarrow d_\downarrow, \quad (1)$$

where summation over the spin indices σ is implied. The fields $\psi_{i\sigma}(x)$ describe chiral, right-moving electrons from lead i, U is the on-site Coulomb repulsion between electrons on the dot, t_i is the coupling between the dot and the lead i, and ϵ_d is the gate voltage. We have set the Fermi velocity $v_F = 1$.

The model's equilibrium properties have been studied in great detail via the traditional thermodynamic Bethe ansatz (TBA).[7,8] The SBA exploits the integrability of the Anderson model to construct current-carrying scattering eigenstates on the open line. There are two main requirements. One is the construction of scattering eigenstates with the number of electrons in each lead conserved prior to scattering off the impurity. Another is the asymptotic boundary condition that the wave functions of the incoming electrons, that is, in the region ($x \ll 0$), tend to those of two free Fermi seas far from the impurity.[25] All information about the external bias applied to the system is encoded in the boundary condition by appropriately choosing the chemical potential of the incoming Fermi seas. As in all Bethe ansatz constructions, the full multiparticle wave function is constructed from single-particle eigenstates (now on the infinite open line) and the appropriate two-particle S matrices. We first rewrite Eq. (1) in the even-odd basis as

$$\begin{aligned}\hat{H} &= \hat{H}_e + \hat{H}_o,\\ \hat{H}_e &= \sum_\sigma \int dx\, \psi^\dagger_{e\sigma}(x)(-i\partial_x)\psi_{e\sigma}(x) + \epsilon_d d^\dagger_\sigma d_\sigma\\ &\quad + t[\psi^\dagger_{e\sigma}(0)d_\sigma + d^\dagger_\sigma \psi_{e\sigma}(0)] + U d^\dagger_\uparrow d_\uparrow d^\dagger_\downarrow d_\downarrow,\\ \hat{H}_o &= \sum_\sigma \int dx\, \psi^\dagger_{o\sigma}(x)(-i\partial_x)\psi_{o\sigma}(x),\end{aligned}$$

with

$$\psi_{e\sigma}(x) = \frac{t_1\psi_{1\sigma}(x) + t_2\psi_{2\sigma}(x)}{\sqrt{t_1^2+t_2^2}},$$
$$\psi_{o\sigma}(x) = \frac{t_2\psi_{1\sigma}(x) - t_1\psi_{2\sigma}(x)}{\sqrt{t_1^2+t_2^2}},$$

and $t = \sqrt{t_1^2+t_2^2}$. In what follows we consider the case $t_1 = t_2 = \frac{t}{\sqrt{2}}$ for simplicity. The single-particle solution for even and odd basis is $|e,p\sigma\rangle = \int dx\, [e^{ipx} g_p(x)\psi^\dagger_{e\sigma}(x) + e_p\delta(x)d^\dagger_\sigma]|0\rangle$ and $|o,p\sigma\rangle = \int dx\, e^{ipx} h_p(x)\psi^\dagger_{o\sigma}(x)|0\rangle$, with $|0\rangle$ the vacuum state and $g_p(x)$, $h_p(x)$, e_p independent of spin and given by

$$\begin{aligned} g_p(x) &= \theta(-x) + e^{i\delta_p}\theta(x) + s_{ep}\,\theta(x)\theta(-x),\\ h_p(x) &= \theta(-x) + \theta(x) + s_{op}\,\theta(x)\theta(-x),\\ e_p &= \frac{t(1+e^{i\delta_p}+s_{ep}/2)}{2(p-\epsilon_d)}.\end{aligned} \quad (2)$$

Here $\delta_p \equiv 2\tan^{-1}(\frac{\Gamma}{\epsilon_d - p})$ is the usual single particle scattering phase shift of the electrons off the impurity obtained when setting $s_{ep} = 0$. $\Gamma \equiv \frac{t^2}{2}$ is the width of the resonance level. We adopted a symmetric regularization scheme $\theta(\pm x)\delta(x) = \frac{1}{2}\delta(x)$ and imposed $|p| \leqslant D$, D being the bandwidth cutoff.[35]

The $s(x) = \theta(x)\theta(-x)$ term appearing in Eqs. (2) and (3) is a local constant since, using our regularization scheme, the locally discontinuous function $s(x)$ satisfies $\partial_x s(x) = [s'(x)|_{x=0^-} + s'(x)|_{x=0^+}]/2 = 0$. It should be noted that this is consistent with the symmetric spread of the δ function around $x = 0$, which is precisely the regularization scheme adopted in this article. Notice also that the single-particle wave functions defined in Eqs. (2) and (3) are properly defined on the whole line $x \in \mathbb{R}$. Considering only half of the domain (such as taking $x > 0$ for instance) would lead to an inconsistency of this regularization. The $s(x)$ term is included in the odd channel function in order to allow for the same two-particle S matrices [Eq. (4)] in all channels.[36,37] The $\theta(x)\theta(-x)$ term in the even channel wave function is introduced in order to modify the original (when $s_{ep} = 0$)

single-particle phase shift across the impurity. The choice of s_{op} and s_{ep} is addressed later. In the lead basis, $|i,p\sigma\rangle$, the single-particle scattering eigenstates with the incoming particle incident from lead i, can be restored by taking a proper linear combination of even-odd states. For example, $|1,p\sigma\rangle = \frac{1}{\sqrt{2}}(|e,p\sigma\rangle + |o,p\sigma\rangle) = \int dx\, e^{ipx}\alpha^{\dagger}_{1,p\sigma}(x)|0\rangle$ is written as

$$|1,p\sigma\rangle = \int dx\, e^{ipx}\left\{[\theta(-x)+\frac{1}{2}(e^{i\delta_p}+1)\theta(x)]\psi^{\dagger}_{1\sigma}(x)+\frac{1}{2}(e^{i\delta_p}-1)\theta(x)\psi^{\dagger}_{2\sigma}(x)+e_p d^{\dagger}_{\sigma}\delta(x)+s^{\dagger}_{1p\sigma}(x)\right\}|0\rangle, \tag{3}$$

with $|2,p\sigma\rangle = \frac{1}{\sqrt{2}}(|e,p\sigma\rangle - |o,p\sigma\rangle) = \int dx\, e^{ipx}\alpha^{\dagger}_{2,p\sigma}(x)|0\rangle$ and $s^{\dagger}_{ip\sigma}(x)$ related to the $\theta(x)\theta(-x)$ terms by

$$s^{\dagger}_{1p\sigma}(x) = \left(\frac{s_{ep}+s_{op}}{\sqrt{2}}\psi^{\dagger}_{1\sigma}(x)+\frac{s_{ep}-s_{op}}{\sqrt{2}}\psi^{\dagger}_{2\sigma}(x)\right)\theta(x)\theta(-x)$$

and

$$s^{\dagger}_{2p\sigma}(x) = \left(\frac{s_{ep}-s_{op}}{\sqrt{2}}\psi^{\dagger}_{1\sigma}(x)+\frac{s_{ep}+s_{op}}{\sqrt{2}}\psi^{\dagger}_{2\sigma}(x)\right)\theta(x)\theta(-x).$$

These states have a single incoming particle ($x<0$) from lead i, which is reflected back into lead i with amplitude $R_p = (e^{i\delta_p}+1)/2$ and transmitted to the opposite lead with amplitude $T_p = (e^{i\delta_p}-1)/2$. Similar single-particle states are discussed in Ref. 25.

The multiparticle Bethe ansatz wave function is constructed by means of the two-particle S matrix, $\mathbf{S}(p,k)$, describing the scattering of two electrons with momenta p and k. By choosing $s_{op} = -4$ in Eq. (2) (the choice of s_{ep} is discussed in Sec. II B and does not affect the result here) in the single particle states we can construct the same two-particle S matrix for all combinations in even-odd basis (see Appendix B). The two-particle solution for both particles coming from lead 1 in spin singlet state takes the following form:

$$\begin{aligned}|1k,\uparrow;1p,\downarrow\rangle &= \int dx_1 dx_2 \mathcal{A}\{e^{i(kx_1+px_2)}Z_{kp}(x_1-x_2)\alpha^{\dagger}_{1k,\uparrow}(x_1)\alpha^{\dagger}_{1p,\downarrow}(x_2)\}|0\rangle \\ &= \Bigg\{\int dx_1 dx_2 A\{g(x_1,x_2)\psi^{\dagger}_{e\uparrow}(x_1)\psi^{\dagger}_{e\downarrow}(x_2)+h(x_1,x_2)\psi^{\dagger}_{o\uparrow}(x_1)\psi^{\dagger}_{o\downarrow}(x_2)+j(x_1,x_2)[\psi^{\dagger}_{e\uparrow}(x_1)\psi^{\dagger}_{o\downarrow}(x_2) \\ &\quad -\psi^{\dagger}_{e\downarrow}(x_1)\psi^{\dagger}_{o\uparrow}(x_2)]\}+\int dx A[e(x)(\psi^{\dagger}_{e\uparrow}(x)d^{\dagger}_{\downarrow}-\psi^{\dagger}_{e\downarrow}(x)d^{\dagger}_{\uparrow}]+o(x)[\psi^{\dagger}_{o\uparrow}(x)d^{\dagger}_{\downarrow}-\psi^{\dagger}_{o\downarrow}(x)d^{\dagger}_{\uparrow})]+Am\, d^{\dagger}_{\uparrow}d^{\dagger}_{\downarrow}\Bigg\}|0\rangle.\end{aligned}$$

Here $\mathcal{A}$ is the antisymmetrizer. A is an overall normalization factor and

$$\begin{aligned}g(x_1,x_2) &= Z_{kp}(x_1-x_2)g_k(x_1)g_p(x_2) \\ &\quad +Z_{kp}(x_2-x_1)g_k(x_2)g_p(x_1),\\ j(x_1,x_2) &= Z_{kp}(x_1-x_2)g_k(x_1)h_p(x_2) \\ &\quad +Z_{kp}(x_2-x_1)h_k(x_2)g_p(x_1),\\ h(x_1,x_2) &= Z_{kp}(x_1-x_2)h_k(x_1)h_p(x_2) \\ &\quad +Z_{kp}(x_2-x_1)h_k(x_2)h_p(x_1),\\ e(x) &= Z_{kp}(-x)g_p(x)e_k + Z_{kp}(x)g_k(x)e_p,\\ o(x) &= Z_{kp}(-x)h_p(x)e_k + Z^{eo}_{kp}(x)h_k(x)e_p,\\ m &= \tilde{Z}_{kp}(0)e_k e_p,\end{aligned}$$

with $Z_{kp}(x) = e^{-i\phi_{kp}}\theta(-x)+e^{i\phi_{kp}}\theta(x)$ and $\tilde{Z}_{kp}(0) \equiv \frac{k+p-2\epsilon_d}{k+p-U-2\epsilon_d}Z_{kp}(0)$. Here $\tan(\phi_{kp}) = \frac{-Ut^2}{(k-p)(p+k-U-2\epsilon_d)}$. The derivation and more general form of two-particle case is written in Appendix B. To include spin triplet case we denote $Z_{k_i,k_j}(x_i-x_j) \equiv Z_{k_i,k_j}(x_i-x_j)^{a_i' a_j'}_{a_i a_j} = \mathbf{I}^{a_i' a_j'}_{a_i a_j}\theta(x_j-x_i)+\mathbf{S}^{a_i' a_j'}_{a_i a_j}(k_i,k_j)\theta(x_i-x_j)$, where a_i is the spin index before the scattering and a_i' the spin index after the scattering. $\mathbf{I}^{a_i' a_j'}_{a_i a_j}$ is the identity matrix. The S matrices must satisfy the Yang-Baxter equations

$$\begin{aligned}&\mathbf{S}^{a_1' a_2'}_{a_1 a_2}(k_1,k_2)\mathbf{S}^{a_1' a_3'}_{a_1 a_3}(k_1,k_3)\mathbf{S}^{a_2' a_3'}_{a_2 a_3}(k_2,k_3) \\ &\quad = \mathbf{S}^{a_2' a_3'}_{a_2 a_3}(k_2,k_3)\mathbf{S}^{a_1' a_3'}_{a_1 a_3}(k_1,k_3)\mathbf{S}^{a_1' a_2'}_{a_1 a_2}(k_1,k_2)\end{aligned}$$

for such a construction to be consistent. The two-particle S matrix for this two-lead Anderson model is given by

$$\mathbf{S}^{a_i' a_j'}_{a_i a_j}(k,p) = \frac{[B(k)-B(p)]\mathbf{I}^{a_i' a_j'}_{a_i a_j}+i2U\Gamma\,\mathbf{P}^{a_i' a_j'}_{a_i a_j}}{B(k)-B(p)+i2U\Gamma}, \tag{4}$$

with $B(k) = k(k-2\epsilon_d-U)$ and $\mathbf{P} = \frac{1}{2}(\mathbf{I}\cdot\mathbf{I}+\vec{\sigma}\cdot\vec{\sigma})$ the spin exchange operator, with a_i and a_j representing the incoming spin indices. Since the S matrix is the same for all even-odd combinations, the S matrix does not depend on the lead index i, and the number of electrons in a lead, N_i, can change only at the impurity site. This circumstance allows us to construct the fully interacting eigenstates of our Hamiltonian characterized by the incoming quantum numbers, N_1 and N_2 the numbers of incident electrons from leads 1 and 2 respectively. These quantum numbers are

subsequently determined by the chemical potentials μ_1 and μ_2, respectively.

To complete the construction of the SBA current-carrying, scattering eigenstate, $|\Psi,\mu_i\rangle$, we must still choose the "Bethe ansatz momenta" $\{p_l\}_{l=1}^{N_1+N_2}$ of the single-particle states to ensure that the incoming particles look like two Fermi seas in the region $x<0$. This requirement translates into a set of "free-field" SBA equations for the Bethe ansatz momenta density of the particles from the two leads.[25] The argument is as follows: Away from the impurity $|i,p\sigma\rangle$ reduces to $\psi^\dagger_{i\sigma}(x)$ with the interparticle S matrix Eq. (4) present. Thus, the scattering eigenstates describing noninteracting electrons are in the Bethe basis rather than in the Fock basis of plane waves. The existence of many bases for the free electron is due to their linear spectrum, which leads to degeneracy of the energy eigenvalues. The wave function $e^{ip_1x_1+ip_2x_2}[\theta(x_1-x_2)+\mathbf{S}\theta(x_2-x_1)]A$ is an eigenstate of the *free* Hamiltonian for any choice of $\mathbf{S}$ with, in particular, $\mathbf{S}=\mathbb{1}$ defining the Fock basis and $\mathbf{S}$ given in Eq. (4) defining the Bethe basis. The Bethe basis is the correct "zero order" choice of a basis in the degenerate energy space required in order to turn on the interactions. We proceed to describe the leads (two free Fermi seas) in this basis.

We consider the system at zero temperature and zero magnetic field in this paper. To describe the two Fermi seas on the leads translates to a set of Bethe ansatz equations whose solution in this case consists of complex conjugate pairs: $p^{\pm}(\lambda)=x(\lambda)\pm iy(\lambda)$ in the λ parametrization,[7,8,38] with

$$x(\lambda)=\tilde{\epsilon}_d-\sqrt{\frac{\lambda+\tilde{\epsilon}_d^2+\sqrt{\left(\lambda+\tilde{\epsilon}_d^2\right)^2+U^2\Gamma^2}}{2}},$$
$$y(\lambda)=-\sqrt{\frac{-\left(\lambda+\tilde{\epsilon}_d^2\right)+\sqrt{\left(\lambda+\tilde{\epsilon}_d^2\right)^2+U^2\Gamma^2}}{2}}, \tag{5}$$

with $\tilde{\epsilon}_d=\epsilon_d+U/2$. Each member of a pair can be either in lead 1 or in lead 2, since the S matrix is unity in the lead space. There are, therefore, two possible configurations for these bound pairs. One possible way of forming bound pairs is described by four types of complex solutions whose densities we denote $\sigma_{ij}(\lambda)$ with $\{ij\}=\{11,12,21,22\}$ indicating the incoming electrons from lead i and lead j. The other possibility, which is perhaps more intuitive in comparing with the free electron in the Fock basis, is to include only $\{ij\}=\{11,22\}$. These two types of states give the same results when evaluating the expectation value of the dot occupation in equilibrium. However, when we turn on the bias voltage, the results obtained from a four-bound-states description show some charge fluctuations even way below the impurity level, which is not expected from the noninteracting ($U\to 0$) theory (shown in Appendix A). Thus, we disregard the four-bound-states solution on physical grounds and focus on the two-bound-states description in the following discussion.

To describe in the Bethe basis the two leads as two Fermi seas filled up to μ_1 and μ_2, respectively, these densities must satisfy the SBA equations,

$$2\sigma_i(\lambda)=-\frac{1}{\pi}\frac{dx(\lambda)}{d\lambda}\theta(\lambda-B_i)-\sum_{j=1,2}\int_{B_j}^{\infty}d\lambda' K(\lambda-\lambda')\sigma_j(\lambda'), \tag{6}$$

with $K(\lambda)=\frac{1}{\pi}\frac{2U\Gamma}{(2U\Gamma)^2+\lambda^2}$.

The SBA equations are derived from imposing boundary condition in the free leads (incoming state) region and the value of momenta is connected with spin rapidity λ by using the quantum inverse scattering method. The Bethe ansatz equations solved with periodic boundary conditions at the free lead region with total number of particles N ($N=N_1+N_2$ as sum of particle number from leads 1 and 2) and the total spin projection S ($S=S_1+S_2=N/2-M$ with $M=M_1+M_2$ as number of down-spin particles from lead 1 and 2) are given by

$$e^{ik_j^l L}=\prod_{\alpha=1}^{M}\frac{B\left(k_j^l\right)-\lambda_\alpha+iU\Gamma}{B\left(k_j^l\right)-\lambda_\alpha-iU\Gamma},$$
$$\prod_{l=1,2}\prod_{j=1}^{N_l}\frac{B\left(k_j^l\right)-\lambda_\alpha-iU\Gamma}{B\left(k_j^l\right)-\lambda_\alpha+iU\Gamma}=\prod_{\beta\neq\alpha}^{M}\frac{\lambda_\alpha-\lambda_\beta+2iU\Gamma}{\lambda_\alpha-\lambda_\beta-2iU\Gamma}, \tag{7}$$

with total energy $E=E_1+E_2$ and $E_l=\sum_j k_j^l$ indicating the energy of the electrons within the lead l at zero temperature.

The spectrum of Eq. (7) for the one-lead case has been analyzed by N. Kawakami and A. Okiji,[8] who found that the ground state at zero temperature is composed of real λ_i and complex k_j^l in the thermodynamic limit for $U>0$. The same situation also occurs in the special limit where $U\to\infty$, where P. Schlottmann[39] has also done the analysis in the one-lead case. The proof that a two-leads ground state is similar to the one-lead case is shown explicitly for the finite temperature calculation and for the infinite-U case in Ref. 38.

As has been mentioned above in the zero-temperature, zero-magnetic-field ground state, all λ_i are real (and distinct) and k_j^l form bound states for $j=1,\ldots,2M$ with bound-state momenta given by the poles or zeros in the S matrix defined in Eq. (4),

$$B[k^{l\pm}(\lambda_j)]=\lambda_j\pm iU\Gamma=B[x(\lambda_j)\pm iy(\lambda_j)]+\gamma^{\pm}(\lambda_j), \tag{8}$$

where $\gamma^{\pm}=O[\exp(-L)]$ and $x(\lambda)$ and $y(\lambda)$ are shown in the Eq. (5).

Note that the bound state can be formed from four possible configurations for $B_2<\lambda_\alpha<\infty$, which we denote bound state from lead i and lead j quasimomenta denoted as λ_α^{ij}. The bound state between $B_1<\lambda_\alpha<B_2$ can only be formed by quasimomenta both coming from lead 1. As already mentioned the four-bound-state distribution does not give physically sensible results for the charge susceptibility as shown in Appendix A and therefore we limit our discussion to two types of bound-state distribution here. Below we surpass the index

of lead in λ and put back the index dependence in the end for simplification. Inserting Eq. (8) into Eq. (7) we get

$$e^{ik_\alpha^+ L} = \prod_{\beta=1}^{M} \frac{\lambda_\alpha - \lambda_\beta + 2iU\Gamma}{\lambda_\alpha - \lambda_\beta + \gamma_\alpha^+}, \tag{9}$$

$$e^{ik_\alpha^- L} = \prod_{\beta=1}^{M} \frac{\lambda_\alpha - \lambda_\beta + \gamma_\alpha^-}{\lambda_\alpha - \lambda_\beta - 2iU\Gamma}, \tag{10}$$

$$\prod_{\beta=1}^{M} \frac{\lambda_\beta - \lambda_\alpha + \gamma_\beta^+}{\lambda_\beta - \lambda_\alpha + \gamma_\beta^-} = 1. \tag{11}$$

Thus, for $L \to \infty$ from multiplication of Eqs. (9) and (10) we have

$$e^{2ix(\lambda_\alpha)L} = \prod_{\beta} \frac{\lambda_\alpha - \lambda_\beta + 2iU\Gamma}{\lambda_\alpha - \lambda_\beta - 2iU\Gamma}. \tag{12}$$

Taking the logarithm of Eq. (12) we have

$$2\pi J_\alpha = -2x(\lambda_\alpha)L - \sum_\beta \left[2\theta_2 \left(\frac{\lambda_\alpha - \lambda_\beta}{2U\Gamma} \right) + \pi \right], \tag{13}$$

with $\theta_n(x) \equiv \tan^{-1}(2x/n)$ and $\{J_\alpha\}$ a set of integer numbers. We can extend the definition of J_α to include integers or half integers and rewrite Eq. (13) as

$$\frac{\pi}{L} J_\alpha = -x(\lambda_\alpha) - \frac{1}{L} \sum_\beta \theta_2 \left(\frac{\lambda_\alpha - \lambda_\beta}{2U\Gamma} \right). \tag{14}$$

Now let us put back the dependence in lead indices. Starting from Eq. (14) it can be shown that there is one-to-one correspondence between the λ_α's and the J_α's and that all λ_α's have to be different. Thus, the set of rapidities $\{\lambda_\alpha^{ij}\}$, characterizing an eigenstate of the Hamiltonian, is uniquely determined by one specific set of $\{J_\alpha\}$. For instance, the ground state of the Hamiltonian H_0 in the presence of a bias voltage is simply obtained by packing two "Fermi seas" of nonconsecutive integers (Pauli principle in lead space) up to certain "Fermi points" (see Fig. 1) corresponding to the B_1 and B_2 in the continuum limit.

For notational simplification we relabel $\{ij\} = \{11,22\}$ as $\{l\} = \{1,2\}$. Now defining $\sum_{ij} \sigma(\lambda_\alpha^{ij}) = \frac{1}{L}\frac{dJ_\alpha}{d\lambda_\alpha} \equiv \sum_l \sigma^{(l)}(\lambda_\alpha)$ and using $\partial_x \theta_n(x) = \frac{2/n}{1+(2x/n)^2}$ we can write Eq. (14) in the continuum limit [by taking $L \to \infty$ and differentiate Eq. (14) with respect to λ]. Doing so we distinguish two different domains:

For $B_2 < \lambda < \infty$ the particles are fully packed and states are labeled by a different lead index l. In this domain, the SBA equations in the continuum limit takes the form

$$\sum_{l=1}^{2} \sigma^{(l)}(\lambda) = -\frac{1}{\pi}\frac{dx(\lambda)}{d\lambda} - \int_{B_2}^{\infty} d\lambda' \, K(\lambda - \lambda')\sigma^{(2)}(\lambda') - \int_{B_1}^{\infty} d\lambda' \, K(\lambda - \lambda')\sigma^{(1)}(\lambda'). \tag{15}$$

For $B_1 < \lambda < B_2$ we can see from Fig. 1 that the lead 2 states are unoccupied. We introduce a distribution of holes for the lead 2 that denote $\tilde{\sigma}^{(2)}(\lambda)$. The continuum SBA equations in this regime are given by

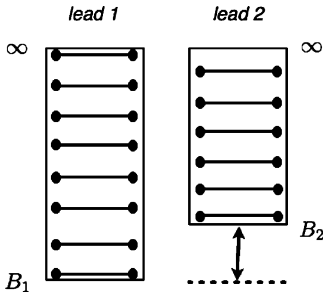

FIG. 1. Sketch of the configuration of Bethe momenta corresponding to the ground state of H_0 with an additional bias voltage, that is, two Fermi seas at different chemical potentials.

$$\sigma^{(1)}(\lambda) + \tilde{\sigma}^{(2)}(\lambda) = -\frac{1}{\pi}\frac{dx(\lambda)}{d\lambda} - \int_{B_2}^{\infty} d\lambda' \, K(\lambda - \lambda')\sigma^{(2)}(\lambda') - \int_{B_1}^{\infty} d\lambda' \, K(\lambda - \lambda')\sigma^{(1)}(\lambda'). \tag{16}$$

Since $\tilde{\sigma}^{(2)}(\lambda)$ obeys the same equation as $\sigma^{(2)}(\lambda)$, as may be seen from subtracting Eqs. (16) and (15), we can combine Eqs. (15) and (16) together to get

$$2\sigma(\lambda) = -\frac{1}{\pi}\frac{dx(\lambda)}{d\lambda} - 2\int_{B_2}^{\infty} d\lambda' \, K(\lambda - \lambda')\sigma(\lambda') - \int_{B_1}^{B_2} d\lambda' \, K(\lambda - \lambda')\sigma(\lambda'), \tag{17}$$

with $B_1 < \lambda < \infty$ for lead 1 and $B_2 < \lambda < \infty$ for lead 2 Bethe momenta-density distributions. Each density is defined in a domain extending from B_i to the cutoff D, to be sent to infinity. The B_i play the role of chemical potentials for the Bethe ansatz momenta and are determined from the physical chemical potentials of the two leads, μ_i, by minimizing the *charge free energy*,

$$F = \sum_i (E_i - \mu_i N_i) = 2\sum_i \int_{B_i}^{\infty} d\lambda \, [x(\lambda) - \mu_i]\sigma_i(\lambda), \tag{18}$$

with σ_1 the lead 1 particle density and σ_2 the lead 2 particle density. Note that σ_1 and σ_2 obey the same integral equation Eq. (6) with different boundary [$\sigma_1(\lambda)$ with $\lambda \subset (B_1,\infty)$ and $\sigma_2(\lambda)$ with $\lambda \subset (B_2,\infty)$]. Solving the SBA equations subject to the minimization of the charge free energy fully determines the current-carrying eigenstate, $|\Psi,\mu_i\rangle$, and allows for calculation of physical quantities by evaluating expectation value of the corresponding operators. In the following we discuss our results from equilibrium cases to nonequilibrium ones, starting with the expression for various expectation values of physical quantities.

B. Expectation value of current and dot occupation

For $\mu_1 = \mu_2$ all B_i are equal to some equilibrium boundary B fixed by the choice of μ_i. The dot occupation is given by the expectation value $\sum_\sigma \langle \Psi,\mu_i | d_\sigma^\dagger d_\sigma | \Psi,\mu_i \rangle$. Taking the limit $L \to \infty$ (L being the size of the lead) one can express n_d as

an integral over the density of λ and the corresponding matrix element $\nu(\lambda) \simeq \frac{\langle p^+(\lambda)p^-(\lambda)|\sum_\sigma d_\sigma^\dagger d_\sigma|p^+(\lambda)p^-(\lambda)\rangle}{\langle p^+(\lambda)p^-(\lambda)|p^+(\lambda)p^-(\lambda)\rangle}$ taken to order $\frac{1}{L}$. Here the state $|p^+(\lambda)p^-(\lambda)\rangle$ denotes a pair (or bound states) of quasiparticles with complex momenta given by Eq. (5). The reason why n_d is governed solely by one-bound-state matrix element instead of a complicated many-particle object is because Bethe wave functions are orthogonal to each other for different pairs of Bethe momenta under the condition that the size of the leads L taken to infinity.

Here we address the different choice of s_{ep} (with $s_{op} = -4$ fixed to have the same S matrix in all channels) which gives rise to different forms of $\nu(\lambda)$. We first discuss the "*natural*" choice $s_{ep} = 0$ [i.e., absence of $\theta(-x)\theta(x)$ terms] and show it reproduces the *exact* result for the dot occupation in equilibrium. While in checking the steady-state condition, that is, $d\langle n_d\rangle/dt = 0$, for the out-of-equilibrium situation, the choice of $s_{ep} = 0$ fails. To remedy this issue we propose $s_{ep} \neq 0$ [i.e., introducing counter-intuitive $\theta(-x)\theta(x)$ terms] schemes to circumvent this difficulty. We check this proposed *phenomenological* scheme in equilibrium against the *exact* dot occupation obtained in the $s_{ep} = 0$ case in the second part of the discussion as a benchmark for our approach. First let us discuss the result for $s_{ep} = 0$.

(1) $s_{ep} = 0$. We choose $s_{ep} = 0$ as in the case of the one-lead Anderson impurity model and denote $\nu(\lambda) = \nu^{SBA}(\lambda)$ in this choice. The dot occupation expectation value in equilibrium is given by

$$\begin{aligned} n_d &= \frac{\langle \Psi, \mu_1 = \mu_2|\sum_\sigma \hat{d}_\sigma^\dagger \hat{d}_\sigma|\Psi, \mu_1 = \mu_2\rangle}{\langle \Psi, \mu_1 = \mu_2|\Psi, \mu_1 = \mu_2\rangle} \\ &= 2\int_B^\infty d\lambda\, \sigma(\lambda)\nu^{SBA}(\lambda), \end{aligned} \tag{19}$$

where the factor 2 in front of the integral accounts for the spin degeneracy. The matrix element of the operator $d_\sigma^\dagger d_\sigma$ in the SBA state is given by

$$\begin{aligned} \nu^{SBA}(\lambda) = &\frac{2\Gamma}{\tilde{x}^2(\lambda) + \tilde{y}_+^2(\lambda)} + \frac{16y(\lambda)\Gamma^2}{[\tilde{x}^2(\lambda) + \tilde{y}_-^2(\lambda)][\tilde{x}^2(\lambda) + \tilde{y}_+^2(\lambda)]} \\ &\times \left(\frac{\tilde{x}(\lambda)}{2\tilde{x}(\lambda) - U}\right)^2, \end{aligned}$$

where we introduced, for simplified notations, the functions $\tilde{x}(\lambda) = x(\lambda) - \epsilon_d$ and $\tilde{y}_\pm(\lambda) = y(\lambda) \pm \Gamma$.

Equation (19) can be proved to be exact by comparing it with the traditional Bethe ansatz (TBA) result. In the latter, n_d is computed as the integral of the impurity density. This observation that the SBA and TBA results for n_d agree in equilibrium shows the connection between the dot occupation and the dressed phase shift across the impurity. The dressed phase shift mentioned here is equivalent to the impurity density as can be seen in the Eq. (C1) in Appendix C. The proof of the equivalence between TBA and SBA in equilibrium is also given in Appendix C.

To describe the out-of-equilibrium state we first check if the steady-state condition $\frac{d\langle \hat{n}_d\rangle}{dt} = 0$ (or equivalently, $\frac{d\langle \hat{N}_1 + \hat{N}_2\rangle}{dt} = 0$) is satisfied in this basis. As mentioned earlier, these scattering states are formed by bound quasiparticles with complex momenta and therefore the single-particle phase across the impurity is not well defined in the sense that $|e^{i\delta_{p^\pm}}| \neq 1$. This problem begins to surface as we set out to evaluate transport expectation value and renders

$$\frac{d\langle \hat{n}_d\rangle}{dt} = \int_{B_{11}}^{B_{22}} d\lambda \sigma_b(\lambda)\Delta(\lambda) \neq 0, \tag{20}$$

with

$$\Delta(\lambda) = \frac{y^2(\lambda)\Gamma^2}{[\tilde{x}^2(\lambda) + \tilde{y}_-^2(\lambda)][\tilde{x}^2(\lambda) + \tilde{y}_+^2(\lambda)]}.$$

Thus, it appears that using this basis the steady-state condition is not observed. This problem does not appear when the momenta are real as in the IRLM case.[25]

(2) $s_{ep} \neq 0$. To remedy this problem we redefine the single-particle phase shifts across the impurity, in analogy to the results for the IRLM,[25] through the choice of nonzero s_{ep} in Eq. (2). With a suitable choice of s_{ep} we may restore a well-defined single-particle phase $|e^{i\tilde{\delta}_{p^\pm}}| = 1$ with $\tilde{\delta}_{p^\pm}$ denoting this new phase. The way we judge whether we make the correct choice for the new phases $\tilde{\delta}_{p^\pm}$ is to compare the dot occupation n_d in equilibrium before and after the redefined phase. The explicit form of s_{ep} and phase $\tilde{\delta}_{p^\pm}$ is motivated below but first we show that a single redefined phase is not sufficient to satisfy the constraint of dot occupation comparison.

Again the choice of new phases is constrained by the requirement that we obtain the same result for $\langle\sum_\sigma d_\sigma^\dagger d_\sigma\rangle$ as given by $\nu^{SBA}(\lambda)$ in equilibrium. Based on this constraint it can be shown explicitly that a single well-defined phase (in the sense of $|e^{i\tilde{\delta}_{p^\pm}}| = 1$) is not sufficient to reproduce the equilibrium $\nu^{SBA}(\lambda)$ as follows: The new dot amplitude $\tilde{e}_{p^+}$ and $\tilde{e}_{p^-}$ have to satisfy

$$\begin{aligned} |\tilde{e}_{p^+}|^2 + |\tilde{e}_{p^-}|^2 &= \frac{4\Gamma}{\tilde{x}^2(\lambda) + \tilde{y}_+^2(\lambda)}, \\ |\tilde{e}_{p^+}|^2|\tilde{e}_{p^-}|^2 &= \frac{4\Gamma^2}{[\tilde{x}^2(\lambda) + \tilde{y}_+^2(\lambda)][\tilde{x}^2(\lambda) + \tilde{y}_-^2(\lambda)]}. \end{aligned}$$

As both $|\tilde{e}_{p^+}|^2$ and $|\tilde{e}_{p^-}|^2$ are positive we see that a single redefined phase cannot satisfy the above constraints simultaneously. Therefore, we have to choose at least two sets of redefined phases $\tilde{\delta}_{p^\pm}^i$ (with $i = s,h$ denoting spin fluctuation or charge fluctuation to be addressed later) and, along with them, some distribution functions f^i to set the weight for these phases.

To motivate the idea of searching the correct phase shifts we come back to the derivation of dot occupation in TBA picture. In TBA the total energy of the system is described by the energy of the leads' electrons and energy shifts from the impurity,

$$E = \sum_j p_j = \sum_j \left(\frac{2\pi n_j}{L} + \frac{1}{L}\delta_j\right). \tag{21}$$

Based on Feynman-Hellman theorem, which is applicable in equilibrium (closed) system, we have

$$\langle \hat{n}_d\rangle = \frac{\partial E}{\partial \epsilon_d} = \frac{1}{L}\sum_j \frac{\partial \delta_j}{\partial \epsilon_d} = \frac{1}{L}\sum_j \frac{\partial\left(\delta_{p_j^+} + \delta_{p_j^-}\right)}{\partial \epsilon_d}. \tag{22}$$

The result for Eq. (2) agrees with those obtained from Eq. (C2) and can be viewed as a third approach to obtain the expectation

value of the dot occupation. The key observation here is that this quantity is related to the *bare* phase shift $\delta_{p^+} + \delta_{p^-}$ and therefore the redefined phases must be proportional to this quantity. Among them there are two likely candidates with redefined phase shift given by $\delta_{p^+} + \delta_{p^-}$, describing the tunneling of a bound pair, and $\frac{\delta_{p^+}+\delta_{p^-}}{2}$, describing the tunneling of a single quasiparticle. In a sense this is the echo for the elementary excitations above the Fermi surface in the Bethe basis characterized by N. Kawakami and A. Okiji[40] as charge-fluctuation excitation, which describes bound-pair-quasiparticle excitation, and spin-fluctuation excitation, which describes one-quasiparticle excitation. Another similar picture is the spin-fluctuation and charge-fluctuation two fluids picture proposed by D. Lee *et al.*[41] albeit in a different context. We identify the phase defined by

$$\tilde{\delta}_{p^-} = \tilde{\delta}_{p^+} = \frac{\delta_{p^+} + \delta_{p^-}}{2} \equiv \tilde{\delta}^s_p$$

[with $s_{ep^\pm} \equiv s^s_{ep^\pm} = \frac{2}{\Gamma}[i(p^\pm - \epsilon_d) - \Gamma](e^{i(\frac{\delta_{p^+}+\delta_{p^-}}{2})} - 1)]$ as spin-fluctuation phase shift and

$$\tilde{\delta}_{p^-} = \tilde{\delta}_{p^+} = \delta_{p^+} + \delta_{p^-} \equiv \tilde{\delta}^h_p$$

[with $s_{ep^\pm} \equiv s^h_{ep^\pm} = \frac{2}{\Gamma}[i(p^\pm - \epsilon_d) - \Gamma](e^{i(\delta_{p^+}+\delta_{p^-})} - 1)]$ as charge-fluctuation phase shift.

The out-of-equilibrium current is evaluated by the expectation value of current operator $\hat{I}$ with $\langle \hat{I} \rangle$ defined by

$$\langle \hat{I} \rangle = \frac{-\sqrt{2}iet}{\hbar} \left\langle \sum_\sigma \{[\psi^\dagger_{1\sigma}(0^\pm) - \psi^\dagger_{2\sigma}(0^\pm)]d_\sigma - \text{H.c.}\} \right\rangle \quad (23)$$

in the state $|\Psi, \mu_i\rangle$. Notice that $\psi^\dagger_{i\sigma}(0^\pm) \equiv \lim_{\epsilon\to 0}[\psi^\dagger_{i\sigma}(-\epsilon) + \psi^\dagger_{i\sigma}(+\epsilon)]/2$ is introduced in transport-related quantity to be consistent with our regularization scheme which introduces another local discontinuity in odd channel at impurity site.

From Eq. (23) and the expression for the phases $\tilde{\delta}^s_p$ and $\tilde{\delta}^h_p$ we have the expression for current as

$$\begin{aligned} I(\mu_1, \mu_2) &= \langle \Psi, \mu_1, \mu_2 | \hat{I} | \Psi, \mu_1, \mu_2 \rangle \\ &= \frac{2e}{\hbar} \int_{B_1}^{B_2} d\lambda\, \sigma_b(\lambda)[f_s(\lambda) J^s(\lambda) + f_h(\lambda) J^h(\lambda)]. \end{aligned} \quad (24)$$

The corresponding spin fluctuation and charge-fluctuation matrix element of the current operator based on the spirit of Landauer transport, denoted as $J^s(\lambda)$ and $J^h(\lambda)$ with $J^\alpha(\lambda) = |T_p(\lambda)|^2 = |\frac{e^{i\tilde{\delta}^\alpha_p} - 1}{2}|^2$ ($\alpha = \{s, h\}$) depending on redefined phase shift $\tilde{\delta}^\alpha_p$ only, are given by

$$J^s(\lambda) = 1 + \frac{\text{sgn}[\tilde{x}(\lambda)][\tilde{x}^2(\lambda) + y^2(\lambda) - \Gamma^2]}{\sqrt{[\tilde{x}^2(\lambda) + y^2(\lambda) - \Gamma^2]^2 + 4\Gamma^2 \tilde{x}^2(\lambda)}} \quad (25)$$

$$J^h(\lambda) = \frac{2\Gamma^2 \tilde{x}^2(\lambda)}{[\tilde{x}^2(\lambda) + \Gamma^2]^2 - 2y^2(\lambda)[\Gamma^2 - \tilde{x}^2(\lambda)] + y^4(\lambda)}. \quad (26)$$

Here $\text{sgn}(x) = \frac{x}{|x|}$ is the sign function. It is introduced in order to pick up the correct branch when taking the square root in the denominator of Eq. (25). This way we ensure that $J^s(\lambda)$ has the proper limit when U is sent to infinity (cf. Sec. III).

Other than the motivations mentioned above for identifying spin and charge fluctuation phase shifts the functional forms of $J^s(\lambda)$ and $J^h(\lambda)$ as a function of bare energy $x(\lambda)$ can also be used to identify these two types of phase shifts (see Fig. 12 in Sec. III for infinite U Anderson model, the finite U is similar).

Next we choose the appropriate weight for each type of phase shift. So far we have not yet been able to deduce the form of these weight functions $f_s(\lambda)$ and $f_h(\lambda)$ and we introduce them *phenomenologically*. Let us define *phenomenological* spin-fluctuation and charge-fluctuation weight functions as

$$f_s[\varepsilon(\lambda)] = \frac{D_s[\varepsilon(\lambda)]}{D_s[\varepsilon(\lambda)] + D_h[\varepsilon(\lambda)]} \quad (27)$$

and

$$f_h[\varepsilon(\lambda)] = \frac{D_h[\varepsilon(\lambda)]}{D_s[\varepsilon(\lambda)] + D_h[\varepsilon(\lambda)]}. \quad (28)$$

Here $D_s[\varepsilon(\lambda)]$ is the spin-fluctuation density of state, $D_h[\varepsilon(\lambda)]$ is the charge-fluctuation density of state as defined in Ref. 40, and $\varepsilon(\lambda)$ is the corresponding dressed energy, that is, the energy required to produce these spin- and charge-fluctuation excitations above the Fermi level. Here dressed energy refers to the sum of the bare energy of adding/removing one bound state, as in charge fluctuation, or single quasiparticle, as in spin fluctuation, and the energy shift from other quasiparticles due to this change. The equation that solves a single quasiparticle's dressed energy $\varepsilon(\lambda)$ reads[42]

$$\varepsilon(\lambda) = [x(\lambda) - \mu] - \int_B^\infty d\lambda'\, K(\lambda - \lambda')\varepsilon(\lambda'). \quad (29)$$

We wish to compare at this point our approach to the one taken by Konik *et al.*[31,32] The authors' Landauer approach is based on an ensemble of renormalized excitations, the holons and spinons, and the conductance is expressed in terms of their phase shift crossing the impurity. However, the leads are built of bare electrons and thus one faces the difficult problem of how to construct a bare electron out of renormalized excitations in order to be able to impose the voltage boundary condition. The basic approximation adopted, electron $\approx$ antiholon + spinon, is valid only when the electron is close to the Fermi surface (see N. Andrei[43]), and therefore the approach is trustworthy only for very small voltages. Nevertheless, the dressed excitations framework seems to give at least qualitatively good results when another energy scale (such as the temperature or an external field) is turned on.[44] In contrast, we construct the eigenstates of the Hamiltonian directly in terms of the bare electron field and can therefore impose the asymptotic boundary condition that the wave function tends to a product of two free Fermi seas composed of bare electrons. While we do not have a mathematically rigorous derivation of the weight functions we introduced, the validity of the scattering formalism is not restricted to any energy window other than energy cutoff.

C. Results for equilibrium and linear response

In the numerical computation, for the practical purpose, we assumed Kondo limit ($U = -2\epsilon_d$, $\frac{U}{\Gamma} \gg 1$) form of the spin-fluctuation and charge-fluctuation distributions, that is,

$$D_s[\varepsilon(\lambda)] \simeq \frac{1}{\pi} \frac{T_k}{\varepsilon^2(\lambda) + T_k^2} \tag{30}$$

and

$$D_h[\varepsilon(\lambda)] \simeq \frac{1}{\sqrt{2U\Gamma}} \frac{\Gamma^2}{[\varepsilon(\lambda) + \epsilon_d]^2 + \Gamma^2}, \tag{31}$$

with T_k being the Kondo scale derived in Ref. 40 as

$$T_k = \frac{\sqrt{2U\Gamma}}{\pi} e^{\pi \frac{\epsilon_d(\epsilon_d+U)+\Gamma^2}{2U\Gamma}}. \tag{32}$$

As we use the Kondo limit in our expression for the spin-fluctuation and charge-fluctuation distributions, we expect that our phenomenological approach works better for large U/Γ. We also take $\varepsilon(\lambda) \simeq x(B) - x(\lambda)$ for numerical convenience with B denoting the Bethe momenta boundary given by $\mu_1 = \mu_2 = 0$. The dot occupation $\langle \sum_\sigma d_\sigma^\dagger d_\sigma \rangle$ evaluated by these new phases is given by

$$\left\langle \sum_\sigma d_\sigma^\dagger d_\sigma \right\rangle = 2\left(\int_{B1}^{\infty} d\lambda\, \sigma_b(\lambda)[\nu^s(\lambda) f_s(\lambda) + \nu^h(\lambda) f_h(\lambda)] + \int_{B_2}^{\infty} d\lambda\, \sigma_b(\lambda)[\nu^s(\lambda) f_s(\lambda) + \nu^h(\lambda) f_h(\lambda)] \right), \tag{33}$$

with $\nu^s(\lambda)$ and $\nu^h(\lambda)$ given as

$$\nu^s(\lambda) = \frac{1}{\Gamma}\left[1 - \frac{[\tilde{x}^2(\lambda) + y^2(\lambda) - \Gamma^2]}{\sqrt{[\tilde{x}^2(\lambda) + y^2(\lambda) - \Gamma^2]^2 + 4\Gamma^2\tilde{x}^2(\lambda)}}\right] \times \left[1 + 8y(\lambda)\frac{1}{\Gamma}\left(1 - \frac{[\tilde{x}^2(\lambda) + y^2(\lambda) - \Gamma^2]}{\sqrt{[\tilde{x}^2(\lambda) + y^2(\lambda) - \Gamma^2]^2 + 4\Gamma^2\tilde{x}^2(\lambda)}}\right)\left(\frac{\tilde{x}(\lambda)}{2\tilde{x}(\lambda) - U}\right)^2\right], \tag{34}$$

$$\nu^h(\lambda) = \left[\frac{2\Gamma\tilde{x}^2(\lambda)}{[\tilde{x}^2(\lambda) + \Gamma^2]^2 - 2y^2(\lambda)[\Gamma^2 - \tilde{x}^2(\lambda)] + y^4(\lambda)}\right] \times \left[1 + \frac{36y(\lambda)\Gamma\tilde{x}^2(\lambda)}{[\tilde{x}^2(\lambda) + \Gamma^2]^2 - 2y^2(\lambda)[\Gamma^2 - \tilde{x}^2(\lambda)] + y^4(\lambda)}\left(\frac{\tilde{x}(\lambda)}{2\tilde{x}(\lambda) - U}\right)^2\right], \tag{35}$$

respectively. We may check whether this choice of *phenomenological distribution functions* satisfies the condition in equilibrium that

$$\left\langle \sum_\sigma d_\sigma^\dagger d_\sigma \right\rangle = 4\int_B^\infty d\lambda\, \sigma_b(\lambda)\nu^{SBA}(\lambda) = 4\left(\int_B^\infty d\lambda\, \sigma_b(\lambda)[\nu^s(\lambda) f_s(\lambda) + \nu^h(\lambda) f_h(\lambda)]\right). \tag{36}$$

We can see from the top of Fig. 2 that the comparison between the phenomenological and the exact result for the dot occupation in equilibrium is good deep into the Kondo regime ($\epsilon_d \simeq -\frac{U}{2}$) and far away from it ($\epsilon_d \gg 0$) but is worse when we are in the mixed valence region ($\epsilon_d \simeq 0$). This discrepancy, due in part to the approximations we made for $D_s(\varepsilon)$ and $D_h(\varepsilon)$, may go away if we took more realistic form of $D_s[\varepsilon(\lambda)]$ and $D_h[\varepsilon(\lambda)]$ also in mixed valence regime, as suggested in Fig. 2. However, the numerical procedure is much more complicated there. We confine ourself to this simpler limit in our phenomenological approach.

Another check on our result in equilibrium is to find the linear response conductance through our formulation and compare with the exact linear result given by the Friedel sum rule.[29,30] The Friedel sum rule, which relates the equilibrium dot occupation to the phase shift experienced by electrons crossing the dot, is related to zero voltage conductance by $\frac{dI}{dV}|_{V=0} = 2\sin^2(\pi\langle\hat{n}_d\rangle/2)$. The zero bias conductance in our construction can be analyzed easily[45] by noting that at low voltage $eV = \mu_1 - \mu_2 \simeq \frac{2\pi}{L}(N_1 - N_2) = 4\pi\int_{B_1}^{B_2}\sigma_b(\lambda)d\lambda$. By taking $B_2 \simeq B_1 = B$ in the expression for the current across the impurity Eq. (24) we get the zero bias conductance expressed as

$$\frac{dI}{dV}\Big|_{V=0} = \frac{e^2}{h}[f_s(B)J^s(B) + f_h(B)J^h(B)]. \tag{37}$$

Here $B = B(\mu, \epsilon_d, \Gamma, U)$ is determined by $\mu_1 = \mu_2 = 0$. The comparison between Friedel sum rule (FSR) result and the conductance given by Eq. (37) [denoted as (pSBA)] is shown at the bottom of Fig. 2. It displays the consequence of the equilibrium Kondo effect in the quantum dot setup: Due to the formation of the Kondo peak attached to the Fermi level, the Coulomb blockade is lifted and a unitary conductance is reached for a range of gate voltages ϵ_d around $-U/2$. Again we see that the comparison is good for large U/Γ but poorer in mixed valence regime for smaller U/Γ, which is consistent with the observation we made when evaluating $\langle\hat{n}_d\rangle$ as shown in top panel of Fig. 2. Having checked our results

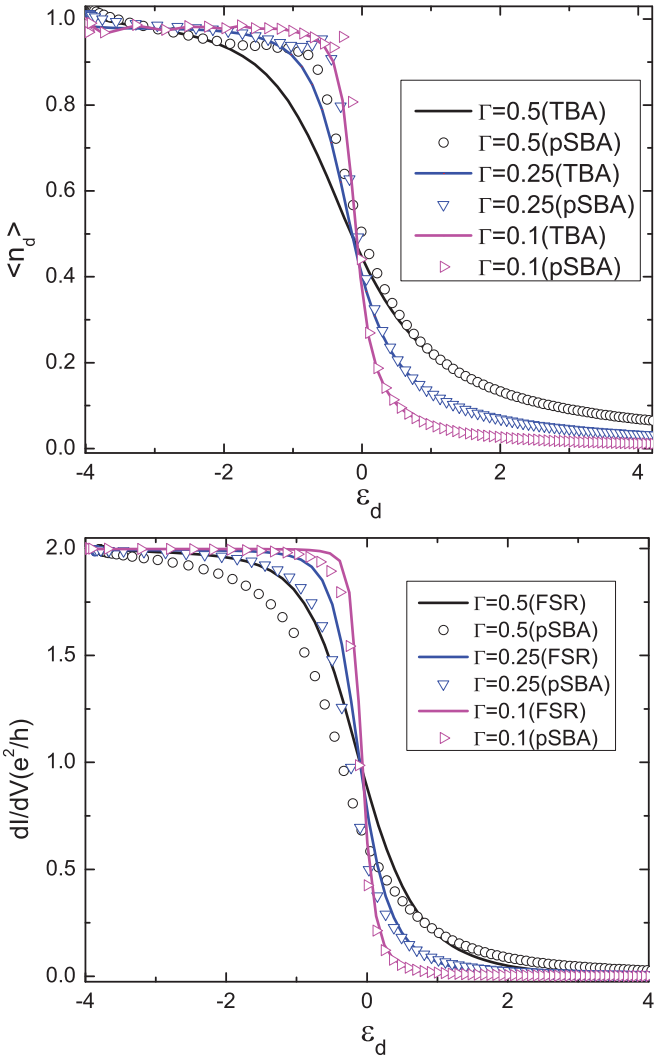

FIG. 2. (Color online) (Top) $\langle \hat{n_d} \rangle$ as a function of ϵ_d from the exact result (solid lines) and from Eq. (36) (symbols). (Bottom) The differential conductance in the linear-response regime, as a function of ϵ_d from the phenomenological scattering Bethe ansatz (pSBA) and exact linear response conductance from Friedel sum rule (FSR) for $\Gamma = 0.5, 0.25, 0.1$, and $U = 8$.

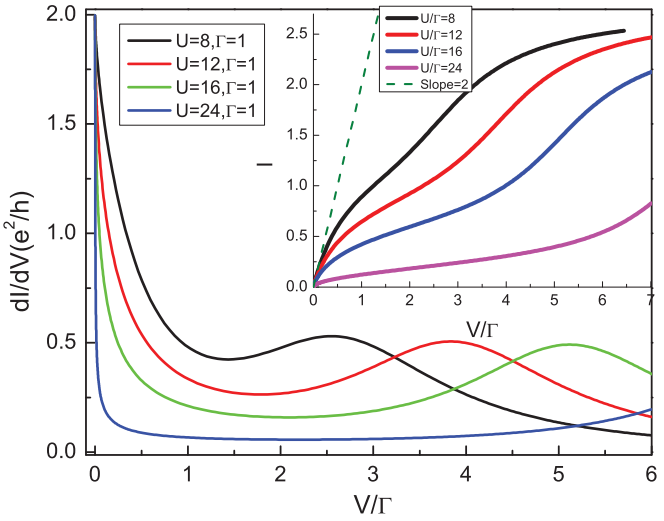

FIG. 3. (Color online) dI/dV vs V/Γ for $\Gamma = 1$, $\epsilon_d = -U/2$, and various U. (Inset) Steady-state current vs voltage curves for $\Gamma = 1$, $\epsilon_d = -U/2$, and various U. The dashed line is a line with constant conductance $\frac{2e^2}{h}$ plotted for comparison.

in equilibrium we go on to compute the current and the dot occupation in the out-of-equilibrium regime.

D. Results out of equilibrium

Now let us begin to investigate the current and dot occupation change as we turn on the voltage. We start with the discussion on current vs voltage for various regime. The current vs voltage is plotted in the inset of figure of Fig. 3 for different values of U and at the symmetric point $\epsilon_d = -U/2$. Note that we use an asymmetric bias voltage when solving numerically the integral equations originating from Eq. (6) with constraint of minimizing the charge free energy Eq. (18): Namely, we fix $\mu_1 \simeq 0$ (around 10^{-3}–10^{-5}) and lower μ_2. Therefore, a direct confrontation between the results obtained from real-time simulations of the Anderson model out of equilibrium[20,21,24] is difficult but the main features of our calculation match the predicted results: a linear behavior of the I-V characteristics at low voltage, the slope being obtained from the FSR (2 in units of e^2/h at the symmetric point), and a nonmonotonic behavior at higher voltage, the so-called nonlinear regime. In particular, our calculations show clearly that the current will decrease as U/Γ is increased, which is in agreement with other numerical approaches (e.g., cf. Fig. 2 of Ref. 21 for a comparison).

The plots of the differential conductance vs source drain voltage for different dot levels, ϵ_d, tunneling strengths Γ, and interaction strengths U are shown in Figs. 3 and 5. Two major features emerge from these plots: (1) a narrow peak around zero bias reaching maximal value of $2e^2/h$ (the unitary limit) for values of the gate voltage close to the symmetric point ($\epsilon_d \simeq -U/2$) and (2) a broader peak developing at finite bias. The first peak is a nonperturbative effect identified as the many-body Kondo peak, characteristic of strong spin fluctuations in the system. However, the broad peak is due to renormalized charge fluctuations around the impurity level. Notice the two features merge as the gate voltage, ϵ_d is raised from the Kondo regime, $\epsilon_d = -U/2$, to the mixed valence regime, $\epsilon_d = 0$, with the Kondo effect disappearing. As a function of the bias the various curves describing the Kondo peak for different values of the parameters can be collapsed onto a single universal function $dI/dV = dI/dV(V/T_k^*)$, as shown in Fig. 4. Here T_k^* is defined as

$$T_k^* = c_1 \frac{\sqrt{2U\Gamma}}{\pi} e^{\frac{\epsilon_d(\epsilon_d+U)+\Gamma^2}{2U\Gamma}}, \tag{38}$$

with $c_1 = 0.002$. The energy scale T_k^* was extracted from the numerics by requiring that the function $dI/dV(V/T_k^*)$ decreases to half its maximal value when $V \simeq T_k^*$. The expression for T_k^*, as given by Eq. (38), differs from the thermodynamic T_k as defined in Eq. (32). The difference of prefactor in the exponential is certainly related to the unusual choice of regularization scheme in the SBA.[35] The other possible implication for this different formulation for

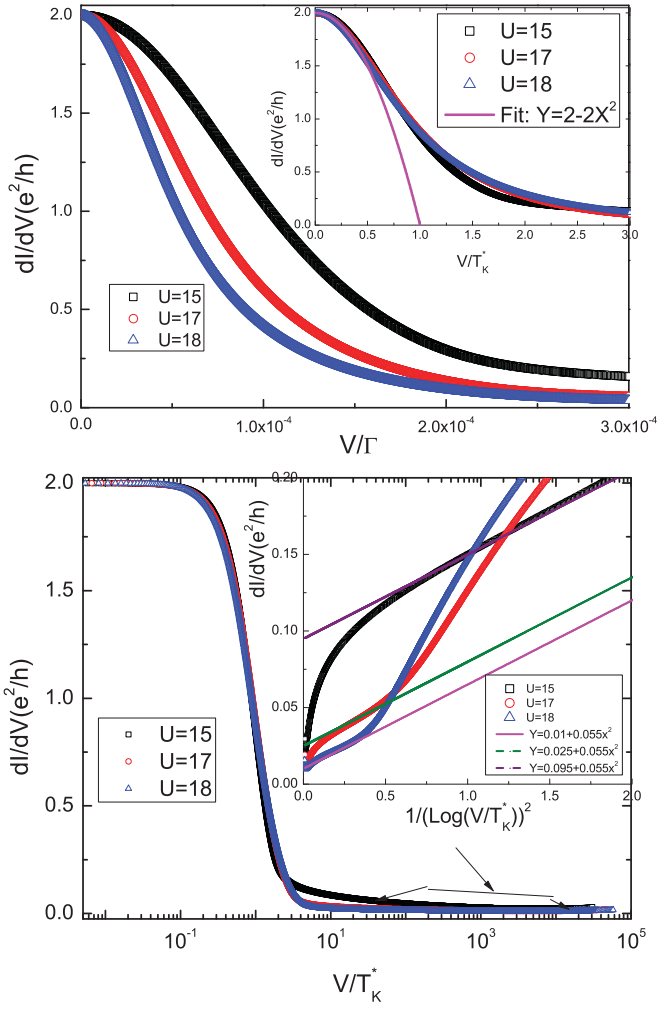

FIG. 4. (Color online) (Top) Zoomed in picture of the differential conductance vs voltage near zero voltage. The inset shows the universality in conductance vs voltage scaled by T_k^* when $\frac{V}{T_k^*} \leqslant 1$. The quadratic behavior occurs for $\frac{V}{T_k^*} < 0.5$ as indicated by the fitted curve. (Bottom) Differential conductance vs voltage scaled by T_k^* near the Kondo peak structure. The inset shows the logarithmic behavior when $\frac{V}{T_k^*} \gg 1$. $\Gamma = 0.5$ for all these data sets.

the Kondo scale is also addressed later when we discuss the experiment done by L. Kouwenhoven *et al.*[5]

The small voltage behavior for differential conductance in symmetric case, that is, $\epsilon_d \simeq -\frac{U}{2}$, is expected to be[12,15]

$$\left.\frac{dI}{dV}\right|_{V \ll T_k^*} \simeq \frac{2e^2}{h}\left[1 - \alpha_V \left(\frac{V}{T_k^*}\right)^2\right]$$

and allows us to identify the constant α_V from the quadratic deviation from $2e^2/h$. The quadratic fit of the universal curve around $V \simeq 0$, as shown in Fig. 4, gives $\alpha_V \simeq 1$. It is also expected for $T_k^* \ll V \ll \frac{U}{2}$ that the tail of the peak decays logarithmically[12] as

$$\frac{dI}{dV} \sim \frac{2e^2}{h}\frac{1}{\ln^2\left(\frac{V}{T_k^*}\right)}.$$

The latter behavior is observed (see inset of Fig. 4) in the regime $\frac{U}{\Gamma} \gg 1$ for $10^2 < \frac{V}{T_k^*} < 10^4$ with the logarithmic

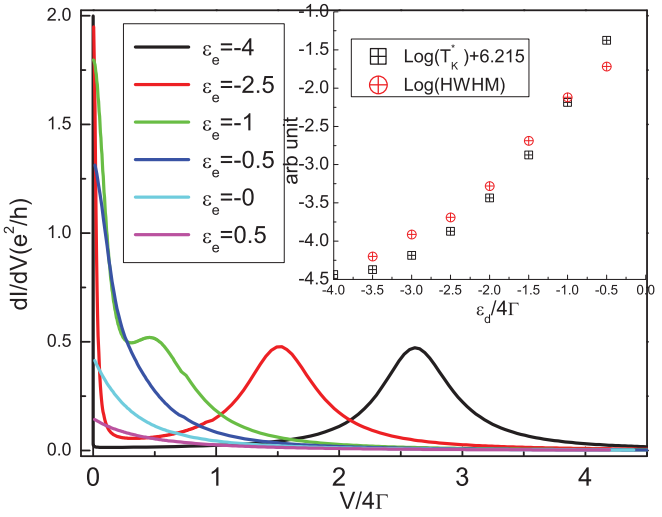

FIG. 5. (Color online) dI/dV vs $V/4\Gamma$ for $U = 8$, $\Gamma = 0.25$ and various ϵ_d from Kondo ($\epsilon_d = -4$) to the mixed-valence regime ($\epsilon_d \simeq 0$). (Inset) Comparison of $\ln(T_k^*) - \ln(c_1)$ and $\ln(V_{HWHM})$ as a function of impurity level ϵ_d. Here V_{HWHM} is the voltage difference estimated at half value of differential conductance at zero voltage. The constant shift $-\ln(c_1)$ is chosen to give the best fit in the data away from $\epsilon_d = -\frac{U}{2}$.

function given by

$$\frac{dI}{dV} = \frac{e^2}{h}\left[f\left(\frac{U}{\Gamma}\right) + \frac{c_2}{\ln^2\left(\frac{V}{T_k^*}\right)}\right],$$

with the parameter $c_2 = 0.055$. Here $f(\frac{U}{\Gamma})$ is simply a constant (in V) shift. As suggested from the bottom plot of Fig. 4 (see also Fig. 14 for the infinite-U case) the charge fluctuation side peak does not fall into the same scaling relation but the strong correlations shift the center of the side peak closer to $V = 0$ (see Figs. 3 and 5). In other words, the position of the resonance in the dI/dV curve naively expected around $V = |\epsilon_d|$ is renormalized[46] by the presence of interactions. In the inset of Fig. 5 we show the logarithm of the voltage obtained at half width at half maximum (HWHM) of the zero voltage peak and compare it with

$$\ln T_k^* = \frac{\epsilon_d(\epsilon_d + U) + \Gamma^2}{2U\Gamma} + \ln\left(c_1 \frac{\sqrt{2U\Gamma}}{\pi}\right)$$

(after subtracting the constant $\ln c_1$). What is important and *universal* is that both quantities ($\ln V_{\rm HWHM}$ and $\ln T_k^*$) exhibit a quadratic behavior in the gate voltage ϵ_d. Similar results had been found experimentally by L. Kouwenhoven *et al.*[5] when they compare the full width at half maximum of dI/dV (from which they obtain a Kondo scale T_{k_1} at finite voltage) with the temperature dependence of the linear response differential conductance (from which another Kondo scale T_{k_2} is extracted). It is suggested from our numerical results that both $\ln T_{k_2}$ (in analogy with our T_k) and $\ln T_{k_1}$ (which is our T_k^*) follow similar quadratic behavior in ϵ_d but differ in their curvatures by a factor of π. In Ref. 5 the curvatures of the quadratic behavior differ by a factor of around 2 [see Fig. 3(B) in Ref. 5], which is attributed to dephasing of spin fluctuations at finite voltage.

Notice that in all the numerical data shown for current vs voltage we have chosen $\frac{U}{\Gamma} \geqslant 8$ to explore the scaling relation in the Kondo regime. Another reason is that our *phenomenological distribution functions* introduced to control the relative weight for spin- and charge-fluctuation contributions work much better in the large $\frac{U}{\Gamma}$ regime (cf. Fig. 2).

Next let us study the change in the dot occupation as a function of the voltage. The extension of the computation of the dot occupation out of equilibrium is straightforward. Suppose we find the correct distribution functions $f_s(\lambda)$ and $f_h(\lambda)$; then we have $\nu^{SBA}(\lambda) = \nu^s(\lambda) f_s(\lambda) + \nu^h(\lambda) f_h(\lambda)$. Under this assumption $\nu^{SBA}(\lambda)$ retains its form in and out of equilibrium and the general expression for $\langle \hat{n}_d \rangle$ is

$$n_d(\mu_1,\mu_2) = \langle \Psi,\mu_1,\mu_2|\hat{n}_d|\Psi,\mu_1,\mu_2\rangle = 2\left(\int_{B_1}^{\infty} d\lambda\, \sigma_b(\lambda)\nu^{SBA}(\lambda) + \int_{B_2}^{\infty} d\lambda\, \sigma_b(\lambda)\nu^{SBA}(\lambda)\right). \tag{39}$$

As the form for $\nu^{SBA}(\lambda)$ is proved to be *exact* in equilibrium, we regard Eq. (39) as an *exact* result for $\langle \hat{n_d} \rangle$ even out of equilibrium and valid in all different ranges of U, ϵ_d, Γ under the *assumption* that the integrand does not change its form for in and out of equilibrium, which is the case for general results of SBA. In the numerical results shown hereafter, we use this expression [Eq. (39)] for the matrix element of dot occupation rather than Eq. (36). We adopt the same voltage drive scheme by fixing μ_1 and lowering μ_2.

By using this result we do not need to confine ourselves to large $\frac{U}{\Gamma}$. The case for different $\frac{U}{\Gamma}$ with $\epsilon_d = -\frac{U}{2}$ and for $U = 8, \Gamma = 0.25$ with different ϵ_d are shown in Figs. 6 and 7. The main features of these plots are a relatively slow decrease of the dot occupation at low voltage followed by an abrupt drop of $\langle n_d \rangle$. The decrease of $\langle n_d \rangle$ takes place within a range of voltage on the order of Γ. Then as we increase the voltage further another plateau develops. Note that, as expected, the bigger U is the higher is the voltage needed to drive the system out of the $\langle n_d \rangle = 1$ plateau. In a sense the charge fluctuations are strongly frozen at large U and it costs more energy to excite them. The voltage where the abrupt drop in $\langle n_d \rangle$ occurs corresponds to the energy scale at which the "charge fluctuation peak" was observed in the conductance plots. This can be seen by comparing the position of the broader peak in Fig. 5 with that of the abrupt dot occupation drop in Fig. 7.

Similar to the differential conductance we may define the *nonequilibrium charge susceptibility* as

$$\chi_c(V)|_{\epsilon_d} = -\frac{\partial \langle \hat{n_d} \rangle}{\partial V},$$

which we obtain by taking a numerical derivative of the dot occupation data with respect to the voltage. In the case of $U = -\epsilon_d/2$ there are two features, as can be seen from the inset of Fig. 6 and main figure of Fig. 7. Near $V \simeq 0$ we see a first small peak arising with width and height decreasing with increasing $\frac{U}{\Gamma}$. We identify this peak as a small remnant of the charge fluctuations in the Kondo regime. This statement is confirmed by noticing that this peak goes away as $\frac{U}{\Gamma}$ increases, vanishing when $U \to \infty$ as shown in Sec. III, where the infinite U Anderson model is discussed. The second peak is located at the same voltage as the charge fluctuation peak observed in the conductance plots and is therefore associated with the response of the renormalized impurity level to the charge susceptibility. This can be seen when comparing Figs. 5 and 7.

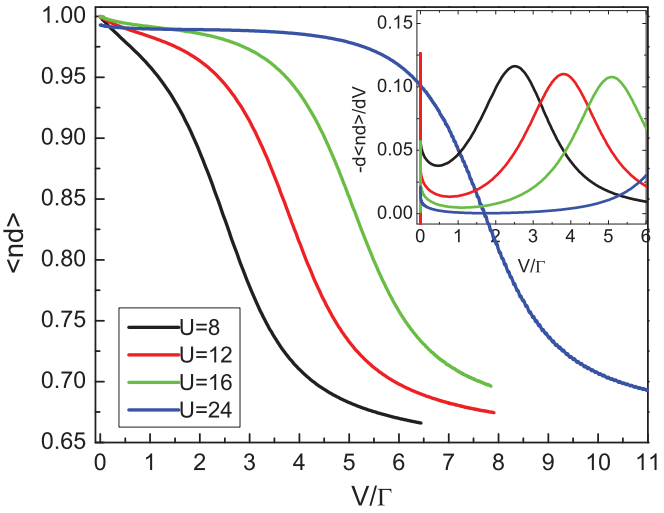

FIG. 6. (Color online) $\langle \hat{n_d} \rangle$ vs V/Γ for different U with $\epsilon_d = -\frac{U}{2}$ and the $\Gamma = 1$ case. (Inset) The corresponding nonequilibrium charge susceptibility. A small peak shows up near $V = 0$ for all these curves.

Another interesting quantity, the usual *charge susceptibility*, defined by $\chi_c(\epsilon_d)|_V = -\frac{\partial \langle \hat{n_d} \rangle}{\partial \epsilon_d}$, can also be qualitatively described. In Fig. 8 we plot $-\frac{\Delta \langle \hat{n_d} \rangle}{\Delta \epsilon_d}$ as a function of ϵ_d as we only have a few points in fixed ϵ_d for finite voltage. Notice that $\chi_c(\epsilon_d)|_V$ tends to be a universal curve in large voltage, indicating charge on the dot remains at some constant value in the steady state with large voltage. This constant value at large voltage, as pointed out by C. J. Bolech, is around 0.65 for the $\epsilon_d = -\frac{U}{2}$ case. In preparing this article we noticed that a similar computation, adopting the same asymmetric voltage drive protocol as we have here, is carried out by R. V. Roermund *et al.*[22] for the dot occupation out of

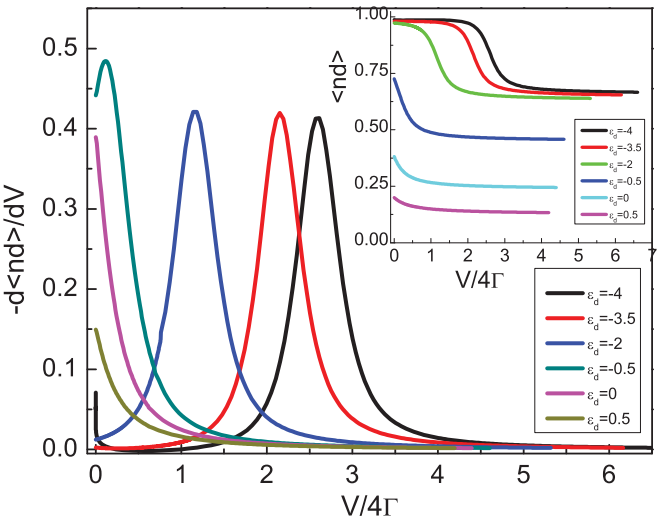

FIG. 7. (Color online) $-\frac{d\langle \hat{n}_d \rangle}{dV}$ vs $V/4\Gamma$ for $\Gamma = 0.25$, $U = 8$, and various ϵ_d from Kondo to the mixed valence regime. We see that the small peak near $V = 0$ only appears when $\epsilon_d \to -\frac{U}{2}$. (Inset) The corresponding $\langle \hat{n_d} \rangle$ vs $V/4\Gamma$.

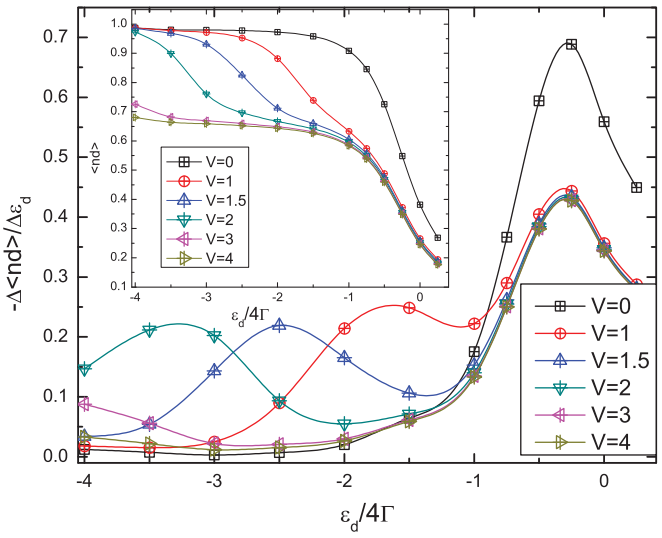

FIG. 8. (Color online) $-\frac{\Delta\langle\hat{n}_d\rangle}{\Delta\epsilon_d}$ for various fixed voltages as a function of ϵ_d for $\Gamma = 0.25$, $U = 8$. (Inset) $\langle\hat{n}_d\rangle$ vs ϵ_d for various fixed voltages.

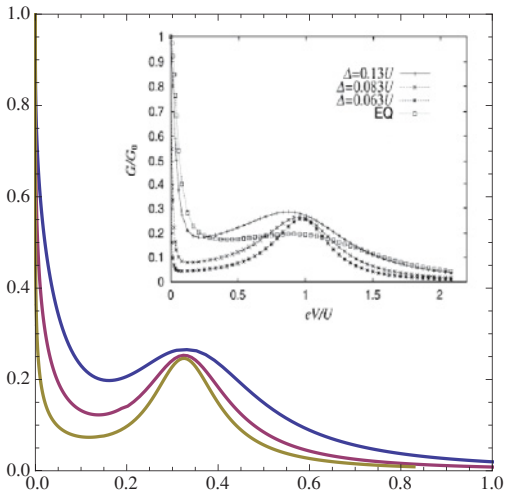

FIG. 9. (Color online) Comparison of our theory with perturbation expansion in U done by D. Matsumoto on dI/dV (y axis in units of $2e^2/h$) vs V/U (x axis). Our data (blue, purple, and brown lines correspond to $\frac{\Gamma}{U} = 0.13$, 0.083, and 0.063, respectively. Δ shown in the inset is Γ in our notation. EQ in the inset is conductance computed by equilibrium density of state which is not relevant to our discussion here.) are shown as the main figure and Fig. 8 in Ref. 23 is shown in the inset. In Ref. 23 the voltage is driven symmetrically, that is, $\mu_1 = -\mu_2$, rendering the factor of two difference in the voltage (i.e., $\frac{V}{U} = 0.5$ in our case corresponds to $\frac{eV}{U} = 1$ in the inset; $e = 1$ in our convention) in comparing our result with that in Ref. 23.

equilibrium by using equation-of-motion method. We do get a similar value for the dot occupation at large voltage. This value is different from the dot occupation value $n_d \simeq 0.5$ at large voltage when the interaction U is turned off, as shown in Fig. 13. This difference might have to do with the 0.7 structure observed in quantum point contact[4] in high temperature (temperature is high compared with the Kondo scale but still small compared with phonon modes or electronic level) and zero magnetic field as the linear response conductance given by $n_d = 0.65$ by using FSR is around 0.73. In a sense the voltage seems to play a similar role as the temperature in the way it influences the dot occupation. Further connection between these two behaviors could be clarified by computing the decoherence factor as in Ref. 22. This decoherence factor is related to the dot correlation function out of equilibrium, which can be computed in a three-lead setup[47] by using our approach.

E. Comparison with other theoretical and experimental results

In most of the other theoretical approaches[17,20–23,31,32] the symmetric voltage drive ($\mu_1 = -\mu_2$) is usually assumed to preserve particle-hole symmetry in symmetric case ($\epsilon_d = -\frac{U}{2}$). It is thus difficult for us to make any definite comparison with other theoretical results. The qualitative feature, as shown by the black curves in Fig. 9 done by D. Matsumoto[23] by using perturbation expansion in U at strong coupling fixed point, is similar to our results in the sense that the height of the charge fluctuation side peak and width are almost the same. The major differences are in the shape of the Kondo peak and the position of the charge fluctuation side peak. A clear signature of renormalized dot level ϵ_d, as hinted in renormalization computation,[46,48] is clearly seen in our result. The shape of Kondo resonance near zero voltage deviates from its quadratic behavior expected from Fermi liquid picture at smaller voltage in our case, as is expected for asymmetric voltage drive.[14,16]

We can also compare our results with experiments. Shown in the inset of Fig. 10 is the $\frac{dI}{dV}$ vs V measured in Co ion transistor by J. Park *et al.*[6] We rescaled the differential conductance and superimposed our numerical results on the data graph. The measurement was done by using an asymmetric drive of the voltage (by keeping $\mu_1 = 0$ and changing μ_2 to be larger or smaller than zero) and thus there is an asymmetry in the differential conductance as a function of voltage as illustrated in the data curve. In our numerics we only compute the scenario for $\mu_1 = 0$ and lowering μ_2 (only for $V > 0$ region of Fig. 10). The $V < 0$ region is plotted by just a reflection with respect to the $V = 0$ axis, which illustrates the case of $\mu_2 = 0$ and lowering μ_1. To compare with the correct voltage setup on the $V < 0$ side as in experiment will involve computations within a different parametrization for the bare Bethe momenta, which is beyond our current scope. The comparison on the $V > 0$ region shows good agreement between our theory and experimental result. The discrepancy on the width of the charge fluctuation side peak could be due to the vibron mode.[49] To describe these types of transistors we start with the Anderson-Holstein Hamiltonian. We are currently exploring the possibility of solving this model by the Bethe ansatz approach.

III. INFINITE U ANDERSON MODEL

In the limit of $\frac{U}{\Gamma} \to \infty$ the finite U two-lead Anderson impurity Hamiltonian becomes the two-lead infinite U Anderson model. The latter model is closely related, via the Schrieffer-Wolff transformation,[50] to the famous Kondo model, a model of spin coupled to a Fermi liquid bath. The

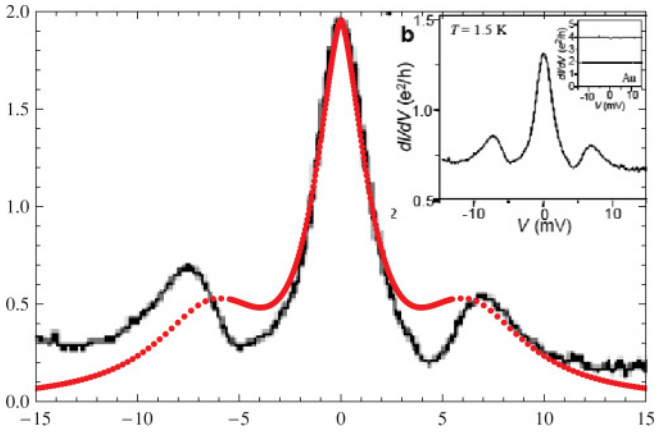

FIG. 10. (Color online) Comparison of theory with experiment of dI/dV (y axis in units of e^2/h) vs V (x axis in units of mV). (Inset) The original data graph published in Ref. 6. The red dots are given by our theory for $\frac{U}{\Gamma} = 8$ with voltage rescaled to fit with original data in units of mV. The value of differential conductance (experiment data in black line) is rescaled from (0.6,1.3) to (0,2) in unit of $\frac{e^2}{h}$.

reason for that is simple: since $U \to \infty$ the charge fluctuations are essentially frozen out and only the spin fluctuations dominate the low-energy physics. The Hamiltonian is given by

$$\hat{H} = \sum_{i=1,2} \int dx\, \psi^\dagger_{i\sigma}(x)(-i\partial_x)\psi_{i\sigma}(x) + \epsilon_d d^\dagger_\sigma d_\sigma + t_i[\psi^\dagger_{i\sigma}(0)b^\dagger d_\sigma + d^\dagger_\sigma b\psi_{i\sigma}(0)]. \tag{40}$$

Here the bosonic operator b is introduced to conserve $b^\dagger b + \sum_\sigma d^\dagger_\sigma d_\sigma = 1$ and by applying the slave boson technique we project out the phase space of double occupancy occurring in finite U case. The corresponding Bethe momenta distribution function for the infinite U Anderson model is given by

$$2\sigma(\Lambda) = \frac{1}{\pi} - \int_{-\infty}^{B_2} d\Lambda' K(\Lambda - \Lambda')\sigma(\Lambda') - \int_{-\infty}^{B_1} d\Lambda' K(\Lambda - \Lambda')\sigma(\Lambda'), \tag{41}$$

with $K(\Lambda) = \frac{1}{\pi}\frac{2\Gamma}{(2\Gamma)^2+(\Lambda-\Lambda')^2}$.

Equation (41) can be derived directly following the procedures in the finite U Anderson model. It can also be derived from the finite U result [Eq. (6)], by taking the large U limit ($U \gg \epsilon_d, U \gg \Gamma$):

$$\begin{aligned}
\frac{x(\lambda)}{U} &\to \frac{1}{2} - \sqrt{\frac{\frac{\lambda}{U^2}+\frac{1}{4}+\sqrt{\left(\frac{\lambda}{U^2}+\frac{1}{4}\right)^2+\frac{\Gamma^2}{U^2}}}{2}} \\
&\to \frac{1}{2} - \sqrt{\frac{\frac{\lambda}{U^2}+\frac{1}{4}+\left|\frac{\lambda}{U^2}+\frac{1}{4}\right|}{2}} \\
&\to \frac{1}{2} - \frac{1}{2}\left(1+\frac{2\lambda}{U^2}+\cdots\right) \to -\frac{\lambda}{U^2} = \frac{\Lambda}{U}, \\
\frac{y(\lambda)}{U} &\to \sqrt{\frac{-\left(\frac{\lambda}{U^2}+\frac{1}{4}\right)+\left[\left(\frac{\lambda}{U^2}+\frac{1}{4}\right)^2+\frac{\Gamma^2}{U^2}\right]^{1/2}}{2}} \\
&\to \sqrt{\frac{\left(\frac{\lambda}{U^2}+\frac{1}{4}\right)\left[-1+\left(1+\frac{\left(\frac{\Gamma}{U}\right)^2}{\left(\frac{\lambda}{U^2}+\frac{1}{4}\right)^2}\right)^{1/2}\right]}{2}} \\
&\to \left(\frac{1}{4}\frac{\left(\frac{\Gamma}{U}\right)^2}{\frac{1}{4}}\right)^{1/2} + \mathcal{O}(U^{-2}) \simeq \frac{\Gamma}{U},
\end{aligned} \tag{42, 43}$$

with $\Lambda \equiv -\frac{\lambda}{U}$. Similar procedures as in Appendix C give the matrix element $\nu^{\rm SBA}_\infty(\Lambda)$ for the dot occupation in the infinite U Anderson model in equilibrium to be

$$\nu^{\rm SBA}_\infty(\Lambda) = \frac{2\Gamma}{(\Lambda-\epsilon_d)^2+(2\Gamma)^2}. \tag{44}$$

In going to the out-of-equilibrium regime ($\mu_1 \neq \mu_2$) we follow the same phenomenological method as for the finite U case. The result for the spin-fluctuation and charge-fluctuation contributions to the dot occupation are given by

$$\begin{aligned}
\nu^s_\infty(\Lambda) &= \frac{1}{\Gamma}\left(1 - \frac{\epsilon_d - \Lambda}{\sqrt{(\epsilon_d-\Lambda)^2+4\Gamma^2}}\right), \\
\nu^h_\infty(\Lambda) &= \frac{2\Gamma}{(\Lambda-\epsilon_d)^2+(2\Gamma)^2}.
\end{aligned} \tag{45}$$

We again check the consistency with the exact result for the dot occupation in equilibrium, namely,

$$\begin{aligned}
\left\langle \sum_\sigma d^\dagger_\sigma d_\sigma \right\rangle &= 4\int_D^B d\Lambda\, \sigma_b(\Lambda)\nu^{\rm SBA}_\infty(\Lambda) \\
&= 4\int_D^B d\Lambda\, \sigma_b(\Lambda)[\nu^s_\infty(\Lambda)f^\infty_s(\Lambda) + \nu^h_\infty(\Lambda)f^\infty_h(\Lambda)].
\end{aligned}$$

Here D is related to the bandwidth and B is determined by the equilibrium Fermi energy $\mu_1 = \mu_2 = 0$. $f^\infty_s(\Lambda)$ and $f^\infty_h(\Lambda)$ are expressed as

$$\begin{aligned}
f^\infty_s(\Lambda) &= \frac{T^\infty_k/\pi}{(\Lambda-B)^2+\left(T^\infty_k\right)^2}, \\
f^\infty_h(\Lambda) &= \frac{2\Gamma}{(\Lambda-B-\epsilon_d)^2+(2\Gamma)^2}.
\end{aligned}$$

Here the Kondo scale T^∞_k used in $f_s(\Lambda)$ takes the form[51]

$$T^\infty_k = \frac{\sqrt{10|D|\Gamma}}{\pi} e^{-\pi\frac{|\epsilon_d|}{\Gamma}}.$$

The results for the dot occupation and FSR check in the infinite U case are shown in Fig. 11. Again we see a nice match between our phenomenological approach and the exact result for $|\frac{\epsilon_d}{\Gamma}| \neq 0$ and some mismatch in the mixed valence region $|\frac{\epsilon_d}{\Gamma}| \simeq 0$. This is consistent with the results for finite U.

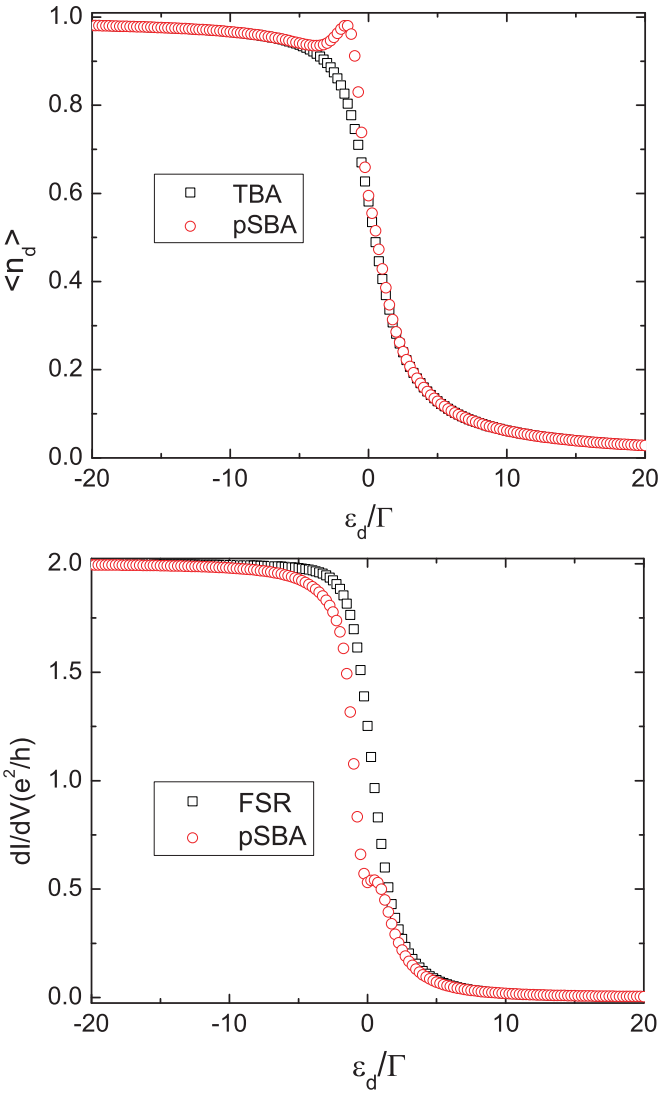

FIG. 11. (Color online) (Top) $\langle \hat{n}_d \rangle$ vs $\frac{\epsilon_d}{\Gamma}$ for exact TBA results and pSBA. (Bottom) Linear response conductance $dI/dV|_{V\to 0}$ vs $\frac{\epsilon_d}{\Gamma}$ for exact result (FSR) and pSBA in the infinite-U Anderson model. $\frac{D}{\Gamma} = -100$. Similar to the case of finite U, the comparison with the nearby mixed-valence region ($\epsilon_d \simeq 0$) is poorer.

The corresponding spin and charge fluctuation matrix element for current, $J^s_\infty(\Lambda)$ and $J^h_\infty(\Lambda)$, are given by

$$J^s_\infty(\Lambda) = 1 - \frac{\epsilon_d - \Lambda}{\sqrt{(\epsilon_d - \Lambda)^2 + 4\Gamma^2}},$$
$$J^h_\infty(\Lambda) = \frac{2\Gamma^2}{(\Lambda - \epsilon_d)^2 + (2\Gamma)^2}. \quad (46)$$

The current expectation value is given by

$$\langle \hat{I} \rangle = \frac{2e}{\hbar} \int_{B_2}^{B_1} d\Lambda \sigma(\Lambda) \left[J^s_\infty(\Lambda) f^\infty_s(\Lambda) + J^h_\infty(\Lambda) f^\infty_h(\Lambda) \right],$$

where B_1 and B_2 are related to μ_1 and μ_2 by minimizing charge free energy F

$$F = 2 \left(\int_D^{B_1} d\Lambda\, \sigma(\Lambda)(\Lambda - \mu_1) + \int_D^{B_2} d\Lambda\, \sigma(\Lambda)(\Lambda - \mu_2) \right).$$

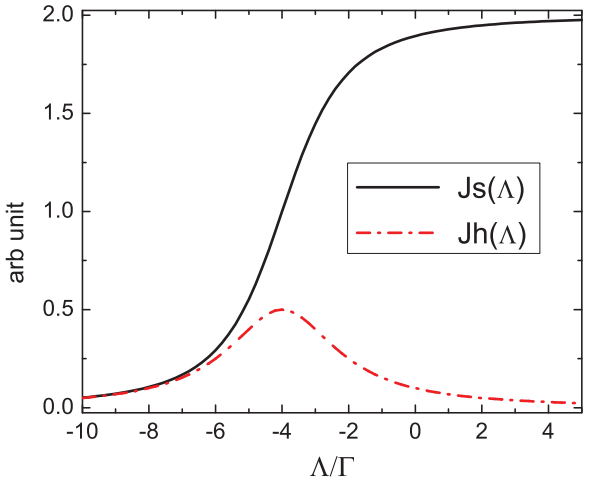

FIG. 12. (Color online) $J_s(\Lambda)$ and $J_h(\Lambda)$ vs Bethe momenta Λ (scaled by Γ) in the infinite-U Anderson model. $\frac{\epsilon_d}{\Gamma} = -4$ in this graph. A similar graph appears for the finite-U case with the x axis replaced by the real part of Bethe momenta $x(\lambda)$.

Before we proceed to discuss the numerical results for current vs voltage in this infinite U model let us look at the structure of $J^s_\infty(\Lambda)$ and $J^h_\infty(\Lambda)$ as a function of Λ as shown in Fig. 12. Λ here represents the bare energy of the quasiparticle and plays the same role as $x(\lambda)$ in the finite U Anderson model. $J^s_\infty(\Lambda)$ alone would reproduce the main feature in the FSR for $\epsilon_d \ll 0$. In this region the linear response conductance comes mainly from the spin fluctuations. The upper plot of Fig. 12 fixes ϵ_d and shows $J^s_\infty(\Lambda)$ vs Λ. We may also fix $\Lambda = 0$ (in the sense of choosing the equilibrium Fermi surface energy at $\Lambda = 0$) and plot $J^s_\infty(\epsilon_d)$ vs ϵ_d. In this way we can see that $J^s_\infty(\epsilon_d)$ vs ϵ_d reproduces the overall structure of the linear response conductance from the Kondo region ($\epsilon_d \leqslant 0$) to the mixed valence regime ($\epsilon_d \simeq 0$). Therefore, we identify the phase shift $\frac{\delta_{p^+} + \delta_{p^-}}{2}$, contributing to $J^s_\infty(\Lambda)$, as the phase shift related to spin fluctuation.

$J^h_\infty(\Lambda)$ gives a Lorentz shape in bare energy scale Λ. This structure is akin to the charge fluctuation side peak with the peak position at energy scale around ϵ_d as seen from the lower plot of Fig. 12. Thus, we identify the phase shift $\delta_{p^+} + \delta_{p^-}$, contributing to $J^h_\infty(\Lambda)$, as the phase shift related to charge fluctuation. These structures also apply to the case of the finite U Anderson model.

Now let us discuss the out-of-equilibrium numerical results. The voltage is again driven asymmetrically by fixing $\mu_1 \simeq 0$ and lowering μ_2. The *exact* dot occupation vs voltage for different ϵ_d for infinite U and $U = 0$, $\frac{\epsilon_d}{\Gamma} = -6$ case (black square dots) are shown in Fig. 13. We see again that the dot occupation decreases slowly at low voltage and develops an abrupt drop at a voltage scale corresponding to impurity level ϵ_d. Also notice the apparent difference between the $U = 0$ plot (black square dots) and the $U \to \infty$ case (red circle dots) and for the same value of $\frac{\epsilon_d}{\Gamma}$. For $U \to \infty$, the dot occupation at large voltage is around 0.65 for $\frac{\epsilon_d}{\Gamma} \ll 0$ which is consistent with the result of the finite U case when $\frac{U}{\Gamma}$ is large (cf. Sec. II D). In contrast, the noninteracting case ($U = 0$) shows that $\langle n_d \rangle \to 0.5$ at large bias.

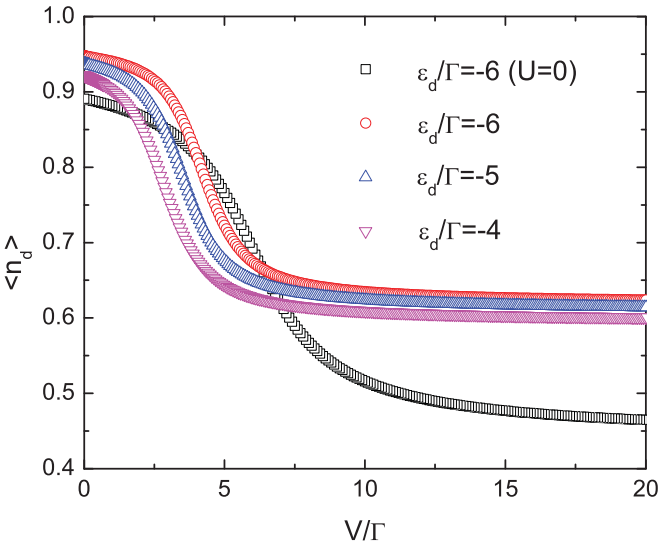

FIG. 13. (Color online) $\langle \hat{n}_d \rangle$ vs $\frac{V}{\Gamma}$ in the infinite-U Anderson model (for red, blue, and purple symbols corresponding to $\frac{\epsilon_d}{\Gamma} = -6, -5, -4$. The black symbols are the $U = 0$ and $\frac{\epsilon_d}{\Gamma} = -6$ case shown for comparison). $\frac{D}{\Gamma} = -100$ in this graph.

The *phenomenological* current vs voltage and the corresponding differential conductance vs voltage are plotted in the top panel of Fig. 14. Again we see the zero bias anomaly and a broad charge fluctuation side peak in the differential conductance vs voltage. The scaling relation of differential conductance vs voltage expected in the small-voltage region can also be extracted by rescaling the voltage by $T_k^{\infty *}$, as shown in bottom figure of Fig. 14. Here $T_k^{\infty *}$ is given by

$$T_k^{\infty *} = \frac{\sqrt{10|D|\Gamma}}{\pi} e^{-\pi \frac{|\epsilon_d|}{2\Gamma}}.$$

Notice that this $T_k^{\infty *}$ differs from T_k^{∞} with a factor of two within the exponent. This factor of two difference represents the difference in the curvature of the parabola as function of ϵ_d (the logarithm of half width at half maximum of the Kondo peak vs ϵ_d shows parabolic curve as in inset of Fig. 6 for finite-U case). This factor of two ratio bears even closer resemblance to the results shown in Ref. 5. Note that in bottom panel of Fig. 14 the positions of the side peak are different and show no universality in that region. It shows universality for $\frac{V}{T_k^*} \leqslant 1$.

IV. CONCLUDING REMARKS

In this article we have explicitly computed the nonequilibrium transport properties in the Anderson model for all voltages using the SBA. In the case of equilibrium we have also shown the equivalence of traditional Bethe ansatz and SBA by evaluating dot occupation in equilibrium. For the expression of current we have introduced *phenomenological distribution functions* to set the weight for spin-fluctuation and charge-fluctuation contributions to the current. The result shows correct scaling relation in Kondo regime as well as satisfying the FSR for linear response for large $\frac{U}{\Gamma}$.

Other interesting quantities, such as the *nonequilibrium charge susceptibility* or the usual charge susceptibility, are

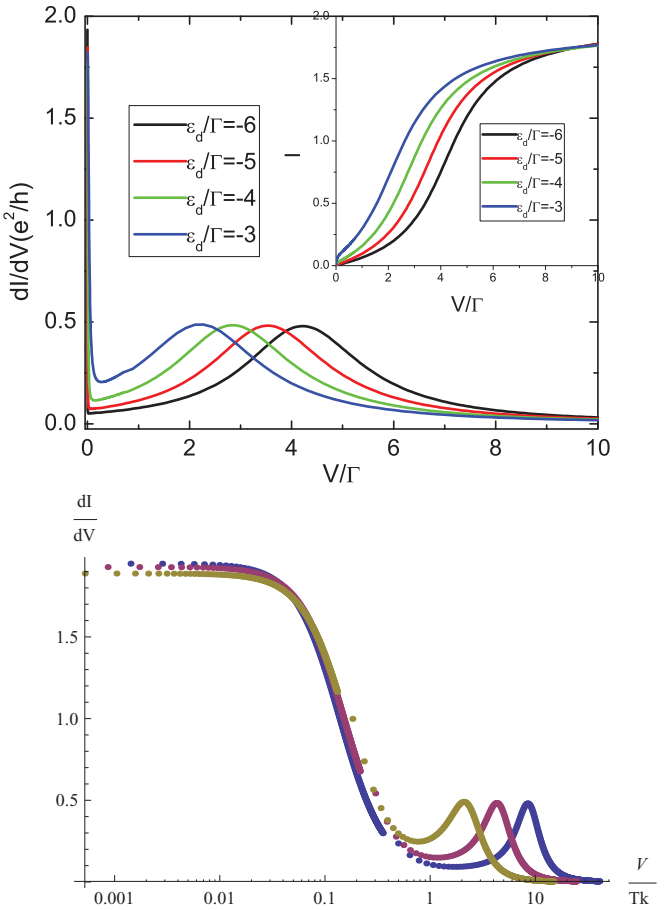

FIG. 14. (Color online) (Top) $\frac{dI}{dV}$ vs $\frac{V}{\Gamma}$ in the infinite-U Anderson model. The inset shows the $I - V$ curves for these parameters. $\frac{D}{\Gamma} = -100$ in this graph. (Bottom) $\frac{dI}{dV}$ vs $\frac{V}{T_k^*}$ shows the scaling relation near zero voltage for $\frac{\epsilon_d}{\Gamma} = -6, -5, -4$ (blue, purple, brown, respectively).

computed numerically via *exact* expression for dot occupation as a function of voltage and impurity level. We believe this report of an *exact* computation of the dot occupation out-of-equilibrium may have interesting application in quantum computing as we understand more the dephasing mechanism. We have also compared our results with perturbation calculation and experimental measurement of nonlinear differential conductance of a quantum dot.

The major difficulty we encounter by using SBA comes from the single-particle phase shift for complex momenta which leads to a breakdown of the steady-state condition when out of equilibrium. One possible issue resulting in this is the local discontinuity at odd channel s_{op}, the choice we made to enable us to construct a scattering state with fixed particles from lead 1 and lead 2. It can be proved that without this choice we cannot write a fixed number of particles incoming from each lead[36] in this Anderson impurity model and similarly for IRLM. The other issue in the study of the Anderson model is whether we shall include all possible bound states in the ground-state construction. From the mathematical structure we choose four types of bound states but the results from charge susceptibility seems to suggest two types of bound states is the correct choice. To check whether this is in general

the correct we plan to come back to study the whole spectrum, which includes the bound state when Bethe energy is higher than the impurity level, of IRLM as this model bares structure similarity to the Anderson model described in this article. Following the SBA on IRLM[25] there are lots of numerical approaches and different exact methods[27] developed for this model and detailed comparison for different approaches is desired for better understanding its physics and scaling relation. By learning how to deal with complex momenta in this model we may also find the rule which may lead us to the *exact* expression for current in this Anderson impurity model.

ACKNOWLEDGMENTS

We are grateful to Kshitij Wagh, Andres Jerez, Carlos Bolech, Pankaj Mehta, Avi Schiller, Kristian Haule, and Piers Coleman for many useful discussions and most particularly to Chuck-Hou Yee for his important help with the numerics and to Natan Andrei for numerous discussions and fruitful ideas. S.P. would also like to thank Daniel Ralph and Joshua Park for permission to use their data and discussion. G.P. acknowledges support from the Stichting voor Fundamenteel Onderzoek der Materie (FOM) in the Netherlands. This research was supported in part by NSF Grant No. DMR-0605941 and a DoEd GAANN fellowship.

APPENDIX A: DISCUSSION OF TWO STRINGS VS FOUR STRINGS

As we have discussed in the main text the bound pair, formed by $p^{\pm}(\lambda) = x(\lambda) \mp iy(\lambda)$, can be formed by quasimomenta from lead 1 or lead 2. We have shown the results for two types of strings (bound states). Namely, the strings are formed by $\{ij\} = \{11,22\}$, with i, j denoting incoming lead indices. In this section we discuss the case of four types of strings and show their corresponding numerical results in the out-of-equilibrium regime. (In equilibrium the two strings and four strings give the same results for dot occupation.)

The density distribution for the Bethe momenta (rapidities) is denoted by $\sigma_{ij}(\lambda)$ with $\{ij\} = \{11,12,21,22\}$ indicating the incoming electrons from lead i and lead j. The $\sigma_{ij}(\lambda)$ is given by

$$4\sigma_{ij}(\lambda) = -\frac{1}{\pi}\frac{dx(\lambda)}{d\lambda} - \sum_{i,j=1,2}\int_{B_{ij}}^{\infty} d\lambda'\, K(\lambda-\lambda')\sigma_{ij}(\lambda'). \tag{A1}$$

The factor of 4 indicates four types of possible configurations and the constraint of exclusions in rapidities λ in solving the quantum inverse scattering problem. The idea is that in equilibrium four types of distributions are equally possible for each bound-state bare-energy $2x(\lambda)$. The B_{ij} play the role of chemical potentials for the Bethe ansatz momenta and are determined from the physical chemical potentials of the two leads, μ_i, by minimizing the charge free energy,

$$F = \sum_i (E_i - \mu_i N_i) = \sum_i \int_{B_{ij}}^{\infty} d\lambda\, [x(\lambda) - \mu_i]\sigma_{(i)}(\lambda) d\lambda,$$

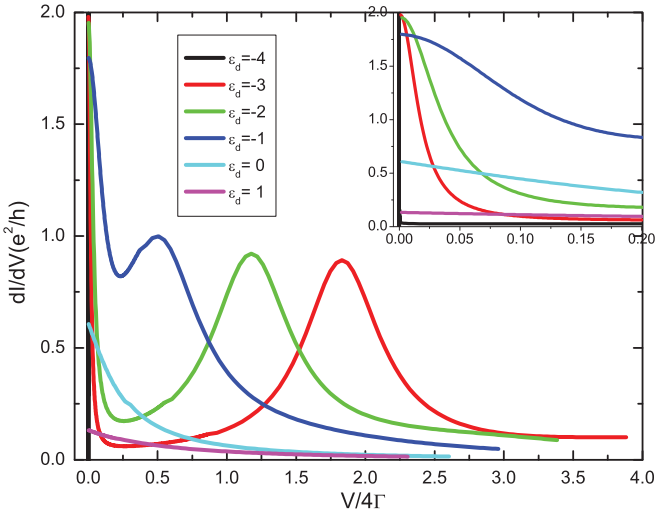

FIG. 15. (Color online) $\frac{dI}{dV}$ vs $\frac{V}{4\Gamma}$ for $U = 8$, $\Gamma = 0.25$, and various ϵ_d from $\epsilon_d = -\frac{U}{2}$ to $\epsilon_d = 1$. The inset is the enlarged region near zero voltage.

with $\sigma_{(1)} \equiv 2\sigma_{11} + \sigma_{12} + \sigma_{21}$ the lead 1 particle density and $\sigma_{(2)} \equiv 2\sigma_{22} + \sigma_{12} + \sigma_{21}$ the lead 2 particle density. In the case of $\mu_1 > \mu_2$ we have $B_{11} < B_{12} = B_{21} < B_{22}$ for this finite-U Anderson model but the equation for $\sigma_{ij}(\lambda)$ is the same for different combinations of i and j. The reason is we use a quasihole state, rather than a quasiparticle state, in the integral equation Eq. (A1) in the treatment of Wiener-Hopf approach. For example, for $B_{11} < \lambda < B_{22}$ there could be three types of quasiparticle state $\{ij\} = \{11,12,21\}$ and we put the $\{ij\} = \{22\}$ state as the quasihole state. This hole state still counts one weight of the probability of four distributions and therefore the factor of 4 on the left-hand side of Eq. (A1) remains even out of equilibrium. A similar idea is also applied in the two types of bound state (strings) solution.

Other than their differences in the density distribution the computations for the current and dot occupation expectation value are quite similar to the two-strings case. We show their numerical results in the following.

The differential conductance vs voltage as shown in Fig. 15, obtained by taking numerical derivative on current vs voltage data, essentially gives the same picture as in the two-strings case, namely, a sharp Kondo peak near $V = 0$ and a broad side peak corresponding to charge fluctuations. In the case of $\langle n_d \rangle$ vs V, however, there is an additional feature occurring at an energy scale higher than the energy scale of the charge fluctuation side peak (corresponding to the voltage position of second peak shown in the inset) as shown in Fig. 16. This is especially apparent if we looked at the nonequilibrium charge susceptibility as shown in the inset of Fig. 16.

As we do not expect there should be any further charge fluctuations, we rule out, by physical argument, the possibility of the four-strings configuration.

APPENDIX B: TWO-PARTICLE SOLUTION AND CHOICE OF s_{op}

For the two-particle solution we follow a similar construction as in P. B. Wiegmann and A. M. Tsvelick's work and the SBA approach developed by P. Mehta and N. Andrei.[24] Since

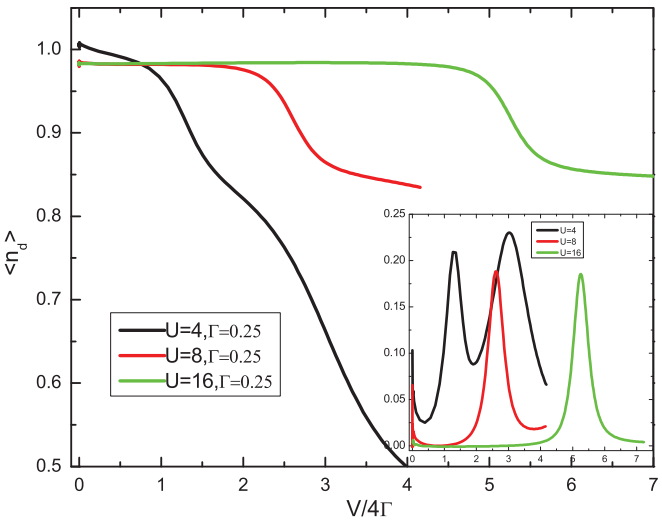

FIG. 16. (Color online) $\langle n_d\rangle$ vs $\frac{V}{4\Gamma}$ for different U, $\Gamma = 0.25$, and $\epsilon_d = -\frac{U}{2}$. The inset is $-\frac{\partial\langle n_d\rangle}{\partial V}|_{\epsilon_d}$ vs V voltage. A third peak shows up in the $U = 4$ case.

Eq. (1) is rotational invariant the spin quantum number is conserved. We show the solution with both particles with spin singlet incoming from lead 1 as an example in the following. Spin quantum number in z direction S_z is a good quantum number and we can write the two-particle solution of the $S_z = 0$ state as

$$|\Psi\rangle = \Big\{ \int dx_1 dx_2 \{ Ag(x_1,x_2)\psi^\dagger_{e\uparrow}(x_1)\psi^\dagger_{e\downarrow}(x_2) + Ch(x_1,x_2) \times \psi^\dagger_{o\uparrow}(x_1)\psi^\dagger_{o\downarrow}(x_2) + Bj(x_1,x_2)[\psi^\dagger_{e\uparrow}(x_1)\psi^\dagger_{o\downarrow}(x_2) - \psi^\dagger_{e\downarrow}(x_1)\psi^\dagger_{o\uparrow}(x_2)]\} + \int dx [Ae(x)(\psi^\dagger_{e\uparrow}(x)d^\dagger_\downarrow - \psi^\dagger_{e\downarrow}(x)d^\dagger_\uparrow] + Bo(x)[\psi^\dagger_{o\uparrow}(x)d^\dagger_\downarrow - \psi^\dagger_{o\downarrow}(x)d^\dagger_\uparrow)] + Amd^\dagger_\uparrow d^\dagger_\downarrow \Big\}|0\rangle.$$

Here A, B, C are arbitrary constants to be determined later. To satisfy $\hat{H}|\Psi\rangle = E|\Psi\rangle = (k+p)|\Psi\rangle$ we have

$$0 = [-i(\partial_{x_1} + \partial_{x_2}) - E]g(x_1,x_2) + t[\delta(x_1)e(x_2) + \delta(x_2)e(x_1)], \quad \text{(B1)}$$

$$0 = [-i(\partial_{x_1} + \partial_{x_2}) - E]h(x_1,x_2), \quad \text{(B2)}$$

$$0 = [-i(\partial_{x_1} + \partial_{x_2}) - E]j(x_1,x_2) + t\delta(x_1)o(x_2), \quad \text{(B3)}$$

$$0 = (-i\partial_x - E + \epsilon_d)e(x) + tg(0,x) + t\delta(x)m, \quad \text{(B4)}$$

$$0 = (-i\partial_x - E + \epsilon_d)o(x) + tj(0,x) \quad \text{(B5)}$$

$$0 = (U + 2\epsilon_d)m + 2te(0) - Em. \quad \text{(B6)}$$

For $U = 0$ the model becomes noninteracting and the two-particle solution becomes a direct product of two one-particle solutions:

$$|\Psi\rangle = |\psi_{k\uparrow}\rangle \otimes |\psi_{p\downarrow}\rangle + |\psi_{p\uparrow}\rangle \otimes |\psi_{k\downarrow}\rangle = \int dx_1 dx_2 \{[g_k(x_1)\psi^\dagger_{e\uparrow}(x_1) + h_k(x_1)\psi^\dagger_{o\uparrow}(x_1) + e_k d^\dagger_\uparrow \delta(x_1)] \times [g_p(x_2)\psi^\dagger_{e\downarrow}(x_2) + h_p(x_2)\psi^\dagger_{o\downarrow}(x_2) + e_p d^\dagger_\downarrow \delta(x_2)] + [g_p(x_1)\psi^\dagger_{e\uparrow}(x_1) + h_p(x_1)\psi^\dagger_{o\uparrow}(x_1) + e_p d^\dagger_\uparrow \delta(x_1)] \times [g_k(x_2)\psi^\dagger_{e\downarrow}(x_2) + h_k(x_2)\psi^\dagger_{o\downarrow}(x_2) + e_k d^\dagger_\downarrow \delta(x_2)]\}|0\rangle.$$

Therefore, at $U = 0$ we have

$$g(x_1,x_2) = g_k(x_1)g_p(x_2) + g_k(x_2)g_p(x_1),$$
$$h(x_1,x_2) = h_k(x_1)h_p(x_2) + h_k(x_2)h_p(x_1),$$
$$j(x_1,x_2) = g_k(x_1)h_p(x_2) + h_k(x_2)g_p(x_1),$$
$$e(x) = e_k g_p(x) + e_p g_k(x),$$
$$o(x) = e_k h_p(x) + e_p h_k(x),$$
$$m = 2e_p e_k.$$

Now for $U \neq 0$ we derive the solution of this form:

$$g(x_1,x_2) = Z_{kp}(x_1 - x_2)g_k(x_1)g_p(x_2) + Z_{kp}(x_2 - x_1)g_k(x_2)g_p(x_1). \quad \text{(B7)}$$

Plugging Eq. (B7) into Eq. (B1) we get

$$e(x) = Z_{kp}(-x)g_p(x)e_k + Z_{kp}(x)g_k(x)e_p. \quad \text{(B8)}$$

Plugging the above two results and Eq. (B4) into Eq. (B6) we get for $m = 2\tilde{Z}_{kp}(0)e_k e_p$

$$[-i\partial_x Z_{kp}(-x)]g_p(x)e_k + [-i\partial_x Z_{kp}(x)]g_k(x)e_p - tZ_{kp}(-x)e_p\delta(x)e_k - tZ_{kp}(x)e_k\delta(x)e_p + 2t\tilde{Z}_{kp}(0)e_k e_p = 0, \quad \text{(B9)}$$

$$2\tilde{Z}_{kp}(0)e_k e_p = \frac{2t[Z_{kp}(0)g_p(0)e_k + Z_{kp}(0)g_k(0)e_p]}{p + k - U - 2\epsilon_d}. \quad \text{(B10)}$$

Now taking $Z_{kp}(x) = e^{-i\phi_{kp}}\theta(-x) + e^{i\phi_{kp}}\theta(x)$ we get $\tan(\phi_{kp}) = \frac{-Ut^2}{(k-p)(p+k-U-2\epsilon_d)}$ and $\tilde{Z}_{kp}(0) = \frac{k+p-2\epsilon_d}{k+p-U-2\epsilon_d}Z_{kp}(0)$. Defining $\Gamma \equiv \frac{t^2}{2}$ and $B(k) \equiv k(k - 2\epsilon_d - U)$ as in Ref. 8 we can rewrite $\tan(\phi_{kp}) = \frac{-2U\Gamma}{[B(k)-B(p)]}$.

From Eq. (B2) we can write $h(x_1,x_2)$ as

$$h(x_1,x_2) = Z^{oo}_{kp}(x_1 - x_2)h_k(x_1)h_p(x_2) + Z^{oo}_{kp}(x_2 - x_1)h_k(x_2)h_p(x_1), \quad \text{(B11)}$$

with arbitrary $Z^{oo}_{kp}(x_1 - x_2)$. Now write $j(x_1,x_2)$ as

$$j(x_1,x_2) = Z^{eo}_{kp}(x_1 - x_2)g_k(x_1)h_p(x_2) + Z^{eo}_{kp}(x_2 - x_1)h_k(x_2)g_p(x_1), \quad \text{(B12)}$$

again with $Z^{eo}_{kp}(x_1 - x_2)$ undetermined. Plugging Eq. (B12) into Eq. (B3) we get $o(x)$ is written as

$$o(x) = Z^{eo}_{kp}(-x)h_p(x)e_k + Z^{eo}_{kp}(x)h_k(x)e_p. \quad \text{(B13)}$$

Now if we choose $Z^{eo}_{kp}(x_1-x_2)=Z_{kp}(x_1-x_2)$ and plug Eqs. (B12) and (B13) into Eq.(B5) we get

$$\begin{aligned}&(-k+\epsilon_d)Z_{kp}(-x)h_p(x)e_k+(-p+\epsilon_d)Z_{kp}(x)h_k(x)e_p\\&\quad+t[Z_{kp}(-x)h_p(x)g_k(0)+Z_{kp}(x)h_k(x)g_p(0)]\\&\quad+(-i)[\partial_x Z_{kp}(-x)]h_p(x)e_k+(-i)[\partial_x Z_{kp}(x)]h_k(x)e_p\\&=-2\sin(\phi_{kp})[h_p(0)e_k-h_k(0)e_p]=0.\end{aligned}\tag{B14}$$

To satisfy Eq. (B14) we can set $h_p(0)=0$ for arbitrary p. This can be done by choosing $s_{op}=-4$ in Eq. (2). Now since $Z^{oo}_{kp}(x_1-x_2)$ is arbitrary we can choose $Z^{oo}_{kp}(x_1-x_2)=Z_{kp}(x_1-x_2)$. Also from Eq. (B10) we have

$$\tilde{Z}_{kp}(0)=\frac{p+k-2\epsilon_d}{p+k-U-2\epsilon_d}Z_{kp}(0).\tag{B15}$$

Since the Hamiltonian in Eq. (1) has rotational invariance the general form of the scattering matrix for particles with momentum k,p and spins a_1,a_2 is given by

$$S^{a_1'a_2'}_{a_1a_2}(k,p)=b(k,p)+c(k,p)\hat{P}^{a_1'a_2'}_{a_1a_2},\tag{B16}$$

where $\hat{P}^{a_1'a_2'}_{a_1a_2}=\frac{1}{2}(1^{a_1'}_{a_1}\cdot 1^{a_2'}_{a_2}+\vec{\sigma}^{a_1'}_{a_1}\cdot\vec{\sigma}^{a_2'}_{a_2})$ is the permutation operator in spins. For antiparallel spins (singlet state), as shown above, $\hat{P}^{a_1'a_2'}_{a_1a_2}=-1$, thus we have

$$\begin{aligned}b(k,p)-c(k,p)&=\frac{Z_{kp}(x>0)}{Z_{kp}(x<0)}\\&=\frac{B(k)-B(p)-i2U\Gamma}{B(k)-B(p)+i2U\Gamma}.\end{aligned}\tag{B17}$$

For the triplet state ($\hat{P}^{a_1'a_2'}_{a_1a_2}=1$) the interaction term with the impurity is absent and the particles passing through each other without changing their phase,

$$b(k,p)+c(k,p)=1.\tag{B18}$$

Thus, from Eqs. (B17) and (B18) we get the two particle S matrix as

$$\hat{S}(k,p)^{a_i'a_j'}_{a_ia_j}=\frac{[B(k)-B(p)]\mathbf{I}^{a_i'a_j'}_{a_ia_j}+i2U\Gamma\mathbf{P}^{a_i'a_j'}_{a_ia_j}}{B(k)-B(p)+i2U\Gamma}.\tag{B19}$$

Thus, the integrability of two leads with the Anderson-type dot system is the similar to the integrability of one lead in the Anderson model.

The choice of identical two-particle S matrices (by choosing $s_{op}=-4$) enables us to construct the scattering state labeled by lead indices by choosing appropriate A,B,C in this even-odd basis. For example, if both particles are coming from lead 1, we choose $(A,B,C)=A_0(\frac{t^2}{t_2^2},\frac{-t^2}{t_1t_2},\frac{t^2}{t_1^2})$ such that the amplitude of the incoming state from lead 2 is zero (A_0 being an overall renormalization constant). We can therefore label the eigenstate by the incoming state from lead i and/or lead j. Without this s_{op} term we cannot write back from the even-odd basis to the lead-indices basis in this two-leads Anderson model and similarly in IRLM in Ref. 25.

APPENDIX C: EQUIVALENCE OF TBA AND SBA IN EQUILIBRIUM

Equation (19) can be proved to be exact by comparing it with the traditional Bethe ansatz where $\langle\sum_\sigma d^\dagger_\sigma d_\sigma\rangle=2\int_B^\infty d\lambda\,\sigma_{\rm imp}(\lambda)$ with impurity density $\sigma_{\rm imp}(\lambda)$ given by

$$\sigma_{\rm imp}(\lambda)=\frac{\delta_{p^+}+\delta_{p^-}}{2\pi}-\int_B^\infty d\lambda'\,K(\lambda-\lambda')\sigma_{\rm imp}(\lambda').\tag{C1}$$

The driving term (first term) of Eq. (C1) is expressed by a bare phase shift $\delta_{p^+}+\delta_{p^-}$ and thus we can view $\sigma_{\rm imp}(\lambda)$ as the dressed phase shift across the impurity. By comparing Eq. (C1) and Eq. (6) in equilibrium [$\sigma_i(\lambda)=\sigma_b(\lambda)$ describing bulk quasiparticle density when $B_1=B_2=B$], we get

$$\begin{aligned}&\int_B^\infty d\lambda\,\sigma_{\rm imp}(\lambda)\left(\frac{-1}{\pi}\frac{dx(\lambda)}{d\lambda}\right)\\&\quad=2\int_B^\infty d\lambda\,\sigma_b(\lambda)\left(\frac{\delta_{p^+}+\delta_{p^-}}{2\pi}\right)\end{aligned}\tag{C2}$$

by noting that the integration kernel $K(\lambda-\lambda')$ is symmetric in λ and λ'. Since the equality is true for arbitrary B we can also rewrite Eq. (C2) as

$$\begin{aligned}\int_B^\infty d\lambda\,\sigma_{\rm imp}(\lambda)&=2\int_B^\infty d\lambda\,\sigma_b(\lambda)\left(\frac{\delta_{p^+}+\delta_{p^-}}{-2\frac{dx(\lambda)}{d\lambda}}\right)\\&\equiv 2\int_B^\infty d\lambda\,\sigma_b(\lambda)\nu^{TBA}(\lambda),\end{aligned}$$

and the resulting $\nu^{TBA}(\lambda)$ is given by

$$\nu^{TBA}(\lambda)=\frac{-\tilde{x}(\lambda)\frac{y'(\lambda)}{x'(\lambda)}-\tilde{y}_-(\lambda)}{\tilde{x}^2(\lambda)+\tilde{y}_+^2(\lambda)}+\frac{\tilde{x}(\lambda)\frac{y'(\lambda)}{x'(\lambda)}+\tilde{y}_+(\lambda)}{\tilde{x}^2(\lambda)+\tilde{y}_+^2(\lambda)}.\tag{C3}$$

Now let us show the computation for $\nu^{\rm SBA}(\lambda)$. First we write the one-particle state of Eq. (1) in the even channel (with $s_{ek}=0$ for the moment) as

$$\begin{aligned}|k,\sigma\rangle&=\int e^{ikx}\alpha^\dagger_{ek,\sigma}(x)dx|0\rangle\\&=\int e^{ikx}\{(\bar{\theta}+A_k\theta)\psi^\dagger_{e\sigma}+B_kd^\dagger_\sigma\delta(x)\}dx|0\rangle.\end{aligned}\tag{C4}$$

Solving $\hat{H}|k,\sigma\rangle=k|k,\sigma\rangle$ we get

$$\begin{aligned}-i(-1+A_k)+B_kt&=0,\\\epsilon_dB_k+t\frac{1+A_k}{2}&=kB_k.\end{aligned}$$

Thus, we get $A_k=\frac{k-\epsilon_d-i\frac{t^2}{2}}{k-\epsilon_d+i\frac{t^2}{2}}$ and $B_k=\frac{t}{k-\epsilon_d+i\frac{t^2}{2}}$. We may also define $g_k(x)=e^{ipx}(\bar{\theta}+A_k\theta)$ and $e_k=B_k$ to have easier comparison with Wiegmann and Tsvelick's work. The two-particle state is obtained by constructing the product of the two-$\alpha^\dagger_{ep,\sigma}(x)$-particle state with the appropriate two-particle S matrix expressed in $Z_{k^+k^-}(x_1-x_2)$.

In principle, we use $|\Psi,N_1,N_2\rangle$ as the many-body state to compute expectation value. However, the simplification here, similar to the case of IRLM in Ref. 25, is that different λ [corresponding to different $p(\lambda)$] are orthogonal to each other in the $L\to\infty$ limit. Thus, the many-body expectation value

can be obtained via two-body computation and the rest just get canceled by the normalization factor. To put it more explicitly, let us denote p_i as the real part of the complex pair $p_i^{\pm}$. Different $|p_i\rangle$ is orthogonal to each other under the condition of size of the leads taken to infinity, or $\frac{\langle p_i|p_j\rangle}{\langle p_i|p_i\rangle} \to 0$ as $L \to \infty$ for $i \neq j$. Thus, the evaluation of the matrix element for operator $\hat{o}$ is given by

$$\frac{\langle p_1, p_2, \ldots, |\hat{o}|p_1, p_2, \ldots\rangle}{\langle p_1, p_2, \ldots, |p_1, p_2, \ldots\rangle} = \sum_{p_i} \frac{\langle p_i|\hat{o}|p_i\rangle}{\langle p_i|p_i\rangle}.$$

Based on this result we demonstrate the explicit computation for dot occupation by two-particle wave functions in the following.

Denote $|\Psi\rangle$ as the two particle solution. We may write spin singlet state as

$$\begin{aligned}
|\Psi\rangle &= \int dx_1 dx_2 \mathcal{A}\{e^{i(kx_1+px_2)} Z_{kp}(x_1-x_2)\alpha^{\dagger}_{ek,\uparrow}(x_1)\alpha^{\dagger}_{ep,\downarrow}(x_2)\}|0\rangle \\
&= \int dx_1 dx_2 \{Z_{kp}(x_1-x_2)[g_k(x_1)g_p(x_2)\psi^{\dagger}_{\uparrow}(x_1)\psi^{\dagger}_{e\downarrow}(x_2) + g_k(x_1)e_p\psi^{\dagger}_{\uparrow}(x_1)d^{\dagger}_{\downarrow}\delta(x_2) \\
&\quad + e_k g_p(x_2)d^{\dagger}_{\uparrow}\delta(x_1)\psi^{\dagger}_{\downarrow}(x_2) + e_k e_p d^{\dagger}_{\uparrow}d^{\dagger}_{\downarrow}\delta(x_1)\delta(x_2)] - Z_{kp}(x_2-x_1)[g_k(x_2)g_p(x_1)\psi^{\dagger}_{e\downarrow}(x_2)\psi^{\dagger}_{e\uparrow}(x_1) \\
&\quad + g_k(x_2)e_p\psi^{\dagger}_{e\downarrow}(x_2)d^{\dagger}_{\uparrow}\delta(x_1) + e_k g_p(x_1)d^{\dagger}_{\downarrow}\delta(x_2)\psi^{\dagger}_{e\uparrow}(x_1) + e_k e_p d^{\dagger}_{\downarrow}d^{\dagger}_{\uparrow}\delta(x_1)\delta(x_2)]\}|0\rangle \\
&= \left\{ \int dx_1 dx_2 [Z_{kp}(x_1-x_2)g_k(x_1)g_p(x_2) + Z_{kp}(x_2-x_1)g_k(x_2)g_p(x_1)]\psi^{\dagger}_{e\uparrow}(x_1)\psi^{\dagger}_{e\downarrow}(x_2) \right. \\
&\quad \left. + \int dx [Z_{kp}(x)g_k(x)e_p + Z_{kp}(-x)g_p(x)e_k][\psi^{\dagger}_{e\uparrow}(x)d^{\dagger}_{\downarrow} - \psi^{\dagger}_{e\downarrow}(x)d^{\dagger}_{\uparrow}] + 2e_k e_p \tilde{Z}_{kp}(0)d^{\dagger}_{\downarrow}d^{\dagger}_{\uparrow} \right\}|0\rangle,
\end{aligned}$$

with $\mathcal{A}$ denoting antisymmetrization and $\tilde{Z}_{kp}(0) = \frac{k+p-2\epsilon_d}{k+p-U-2\epsilon_d} Z_{kp}(0)$.

Solving $\hat{H}|k,\sigma; p, -\sigma\rangle = (k+p)|k,\sigma; p, -\sigma\rangle$, we obtain

$$Z_{kp}(x_1-x_2) = \theta(x_1-x_2) + \frac{(k-p)(k+p-2\epsilon_d-U) - iUt^2}{(k-p)(k+p-2\epsilon_d-U) + iUt^2}\theta(x_2-x_1).$$

For the case of bound states the two-particle S matrix is given by $Z_{k^+k^-}(x_1-x_2) = \theta(x_1-x_2) \equiv \theta^x_{12}$. The normalization factor and matrix element of dot occupation given by the even channel two-particle wave function are

$$\begin{aligned}
\langle\Psi|\Psi\rangle &= \int dy_1 dy_2 \int dx_1 dx_2 \left[\theta^y_{12} g_{k^+}(y_1)g_{k^-}(y_2) + \theta^y_{21} g_{k^+}(y_2)g_{k^-}(y_1)\right]^* \\
&\quad \times \left[\theta^x_{12} g_{k^+}(x_1)g_{k^-}(x_2) + \theta^x_{21} g_{k^+}(x_2)g_{k^-}(x_1)\right]\delta(x_1-y_1)\delta(x_2-y_2) + 2\int dy \int dx [\theta(y)g_{k^+}(y)e_{k^-} \\
&\quad + \theta(-y)g_{k^-}(y)e_{k^+}]^*[\theta(x)g_{k^+}(x)e_{k^-} + \theta(-x)g_{k^-}(x)e_{k^+}]\delta(x-y) \\
&\quad + 4[e_{k^+}e_{k^-}\tilde{Z}_{k^+k^-}(0)]^*[e_{k^+}e_{k^-}\tilde{Z}_{k^+k^-}(0)], \\
\sum_{\sigma}\langle\Psi|\hat{d}^{\dagger}_{\sigma}\hat{d}_{\sigma}|\Psi\rangle &= 2\int dy \int dx [\theta(y)g_{k^+}(y)e_{k^-} + \theta(-y)g_{k^-}(y)e_{k^+}]^*[\theta(x)g_{k^+}(x)e_{k^-} + \theta(-x)g_{k^-}(x)e_{k^+}]\delta(x-y) \\
&\quad + 8[e_{k^+}e_{k^-}\tilde{Z}_{k^+k^-}(0)]^*[e_{k^+}e_{k^-}\tilde{Z}_{k^+k^-}(0)] \\
&= 2\left\{ \int dx [\theta(x)|g_{k^+}(x)e_{k^-}|^2 + \theta(-x)|g_{k^-}(x)e_{k^+}|^2] + 4|e_{k^+}e_{k^-}\tilde{Z}_{k^+k^-}(0)|^2 \right\}.
\end{aligned}$$

Note that the even-channel bound state can be written as sum over the bound state of {11,12,21,22} (four-strings type) or {11,22} (two-strings type) with the same real part of energy $k = x(\lambda)$. This can be viewed as the consistency counting from the Fock basis to the Bethe basis as electrons in lead 1 and lead 2 has fourfold degeneracies in its initial state (two different spins in each lead). Also note that

$$\begin{aligned}
\int dx_1 dx_2\, \theta^x_{12}|g_{k^+}(x_1)g_{k^-}(x_2)|^2 &= \int dx_1 dx_2 |e^{i(k^+x_1+k^-x_2)}(\bar{\theta}_1 + \theta_1 A_{k^+})(\bar{\theta}_2 + \theta_2 A_{k^-})|^2\theta_{12} \\
&= \int dx_1 dx_2\, e^{-2\xi_k(x_1-x_2)}|\bar{\theta}_1\bar{\theta}_2\theta_{12} + \theta_1\bar{\theta}_2\theta_{12}A_{k^+} + \theta_1\theta_2\theta_{12}A_{k^+}A_{k^-}|^2 \\
&= \left(\frac{L}{2\xi_k} - \frac{1-e^{-2\xi_k L}}{(2\xi_k)^2}\right)\left(1 + |A_{k^+}A_{k^-}|^2\right) + \left(\frac{1-e^{-2\xi_k L}}{2\xi_k}\right)^2 |A_{k^+}|^2,
\end{aligned}$$

$$\int dx\,\theta(x)|g_{k^+}(x)e_{k^-}|^2 = \int dx\,\theta(x)|e^{i(k+i\xi_k)x}[\theta(-x)+A_{k^+}\theta(x)]e_{k^-}|^2 = \int_0^L dx\,e^{-2\xi_k x}|A_{k^+}e_{k^-}|^2$$
$$= \frac{1}{2\xi_k}\left|\frac{k-\epsilon_d+i\xi_k-i\Gamma}{k-\epsilon_d+i\xi_k+i\Gamma}\frac{t}{k-\epsilon_d-i\xi_k+i\Gamma}\right|^2 = \frac{1}{2\xi_k}\left|\frac{t}{k-\epsilon_d+i\xi_k+i\Gamma}\right|^2,$$
$$\int dx\,\theta(-x)|g_{k^-}(x)e_{k^+}|^2 = \int dx\,\theta(-x)|e^{i(k-i\xi_k)x}[\theta(-x)+A_{k^-}\theta(x)]e_{k^+}|^2 = \int_{-L}^0 dx\,e^{2\xi_k x}|A_{k^-}e_{k^+}|^2$$
$$= \frac{1}{2\xi_k}\left|\frac{t}{k-\epsilon_d+i\xi_k+i\Gamma}\right|^2,$$

with $\tilde{Z}_{k^+k^-}(0) = \frac{2(k-\epsilon_d)}{2(k-\epsilon_d)-U}Z_{k^+k^-}(0)$ and $Z_{k^+k^-}(0) = \frac{1}{2}$ based on our regularization scheme. By expressing $k = x(\lambda)$ and $\xi_k = y(\lambda)$ and taking $L \to \infty$, thus preserving $\frac{1}{L}$ terms only, we get

$$\frac{\langle\Psi|\sum_\sigma \hat{d}_\sigma^\dagger\hat{d}_\sigma|\Psi\rangle}{\langle\Psi|\Psi\rangle} = \frac{1}{L}\nu^{\mathrm{SBA}}(\lambda) \tag{C5}$$
$$= \frac{1}{L}\left\{\frac{2\Gamma}{\tilde{x}^2(\lambda)+\tilde{y}_+^2(\lambda)} + \frac{16y(\lambda)\Gamma^2}{[\tilde{x}^2(\lambda)+\tilde{y}_-^2(\lambda)][\tilde{x}^2(\lambda)+\tilde{y}_+^2(\lambda)]}\left(\frac{\tilde{x}(\lambda)}{2\tilde{x}(\lambda)-U}\right)^2\right\}.$$

By expressing $\nu^{TBA}(\lambda)$ and $\nu^{\mathrm{SBA}}(\lambda)$ in λ explicitly we see that $\nu^{TBA}(\lambda) = \nu^{\mathrm{SBA}}(\lambda)$. Since $\langle\sum_\sigma d_\sigma^\dagger d_\sigma\rangle = 2\int_B^\infty d\lambda\sigma_{\mathrm{imp}}(\lambda)$ in TBA we have proved that the expectation value evaluated by the state we constructed is exact and the equivalence of SBA and TBA in equilibrium in this two-lead Anderson model.

[1] D. Goldhaber-Gordon, H. Strickman, D. Mahalu, D. Abusch-Magder, U. Meirav, and M. A. Kastner, Nature (London) **391**, 156 (1998); M. Grobis, I. G. Rau, R. M. Potok, H. Shtrikman, and D. Goldhaber-Gordon, Phys. Rev. Lett. **100**, 246601 (2008).

[2] J. Schmid, J. Weis, K. Eberl, and K. Von Klitzing, Physica B **258**, 182 (1998).

[3] S. M. Cronenwett, T. H. Oosterkamp, and L. P. Kouwenhoven, Science **281**, 540 (1998).

[4] S. M. Cronenwett, H. J. Lynch, D. Goldhaber-Gordon, L. P. Kouwenhoven, C. M. Marcus, K. Hirose, N. S. Wingreen, and V. Umansky, Phys. Rev. Lett. **88**, 226805 (2002).

[5] W. G. van der Wiel, S. De Franceschi, T. Fujisawa, J. M. Elzerman, S. Tarucha, and L. P. Kouwenhoven, Science **289**, 2105 (2000).

[6] J. Park, A. N. Pasupathy, J. I. Goldsmith, C. Chang, Y. Yaish, J. R. Petta, M. Rinkoski, J. P. Sethna, H. D. Abruna, P. L. McEuen, and D. C. Ralph, Nature (London) **417**, 722 (2002).

[7] P. B. Wiegman and A. M. Tsvelik, J. Phys. C **16**, 2281 (1983); Adv. Phys. **32**, 453 (1983).

[8] N. Kawakami and A. Okiji, J. Phys. Soc. Jpn. **51**, 1145 (1982); Solid State Commun. **43**, 365 (1982).

[9] T. K. Ng and P. A. Lee, Phys. Rev. Lett. **61**, 1768 (1988).

[10] L. I. Glazman and M. E. Raikh, Pis'ma Zh. Eksp. Teor. Fiz. **47**, 378 (1988) [JETP Lett. **47**, 452 (1988)].

[11] N. Wingreen and Y. Meir, Phys. Rev. B **49**, 11040 (1994).

[12] M. Pustilnik and L. I. Glazman, Phys. Rev. Lett. **87**, 216601 (2001).

[13] M H. Hettler and H. Schoeller, Phys. Rev. Lett. **74**, 4907 (1995).

[14] A. Oguri, Phys. Rev. B **64**, 153305 (2001).

[15] A. Oguri, J. Phys. Soc. Jpn. **74**, 110 (2005).

[16] Z. Ratiani and A. Mitra, Phys. Rev. B **79**, 245111 (2009).

[17] A. Rosch, J. Kroha, and P. Wölfle, Phys. Rev. Lett. **87**, 156802 (2001).

[18] K. S. Thygesen and A. Rubio, Phys. Rev. B **77**, 115333 (2008).

[19] L. G. G. V. Dias da Silva, F. Heidrich-Meisner, A. E. Feiguin, C. A. Busser, G. B. Martins, E. V. Anda, and E. Dagotto, Phys. Rev. B **78**, 195317 (2008).

[20] J. Eckel, F. Heidrich-Meisner, S. G. Jakobs, M. Thorwart, M. Pletyukhov, and R. Egger, New J. Phys. **12**, 043042 (2010).

[21] F. Heidrich-Meisner, A. E. Feiguin, and E. Dagotto, Phys. Rev. B **79**, 235336 (2009).

[22] R. V. Roermund, S.-Y. Shiau, and M. Lavagna, Phys. Rev. B **81**, 165115 (2010).

[23] D. Matsumoto, J. Phys. Soc. Jpn. **69**, 1449 (2000).

[24] C. D. Spataru, M. S. Hybertsen, S. G. Louie, and A. J. Millis, Phys. Rev. B **79**, 155110 (2009).

[25] P. Mehta and N. Andrei, Phys. Rev. Lett. **96**, 216802 (2006); **100**, 086804 (2008). See also e-print arXiv:cond-mat/0702612 (to be published) for more detailed discussion of techniques of SBA and e-print arXiv:cond-mat/0703426 (to be published).

[26] A. Schiller and N. Andrei, e-print arXiv:0710.0249 (to be published).

[27] E. Boulat and H. Saleur, Phys. Rev. B **77**, 033409 (2008).

[28] E. Boulat, H. Saleur, and P. Schmitteckert, Phys. Rev. Lett. **101**, 140601 (2008).

[29] J. S. Langer and V. Ambegaokar, Phys. Rev. **121**, 1090 (1961).

[30] D. C. Langreth, Phys. Rev. **150**, 516 (1966).

[31] R. M. Konik, H. Saleur, and A. W. W. Ludwig, Phys. Rev. Lett. **87**, 236801 (2001).

[32] R. M. Konik, H. Saleur, and A. Ludwig, Phys. Rev. B **66**, 125304 (2002).

[33] P. Fendley, A. W. W. Ludwig, and H. Saleur, Phys. Rev. B **52**, 8934 (1995).

[34] P. Fendley, A. W. W. Ludwig, and H. Saleur, Phys. Rev. Lett. **74**, 3005 (1995).

[35] A renormalizable Hamiltonian such as the Anderson model requires regularization and a cutoff scheme to define it. The results are universal once the cutoff is removed. In intermediate stages as the cut off is finite it is important to adopt a scheme that does not break integrability. The scheme adopted here satisfies this requirement. See N. Andrei, K. Furuya, and J. H. Lowenstein, Rev. Mod. Phys. **55**, 331 (1983), Sec. VI.

[36] Without the regularization factor in the odd sector the model is still integrable. However, it is not possible to identify the fixed number of incoming particles by this choice, A. Nishino and N. Hatano, J. Phys. Soc. Jpn. **76**, 063002 (2007).

[37] It is also possible to construct scattering eigenstate not in the Bethe ansatz form. See J. T. Shen and S. Fan, Phys. Rev. Lett. **98**, 153003 (2007); A. Nishino, T. Imamura, and N. Hatano, *ibid.* **102**, 146803 (2009) for IRLM, and the two-particle state for Anderson model in T. Imamura, A. Nishino, and N. Hatano, Phys. Rev. B **80**, 245323 (2009). It is, however, difficult to find a consistent way to write an N-particles eigenstate through this approach.

[38] The TBA proof of ground-state configuration for two leads case was done by C. J. Bolech and then by S. P. Chao. The idea is to write down finite-temperature free energy for two leads system at different chemical potentials and find the lowest energy state as temperature is taken to zero. The ground state is shown to be formed by complex solutions originated from poles (zeros) of two particle S matrices. For details, see S. P. Chao, Ph.D. thesis, Rutgers University, 2010.

[39] P. Schlottmann, Z. Phys. B **52**, 127 (1983).

[40] N. Kawakami and A. Okiji, Phys. Rev. B **42**, 2383 (1990).

[41] D. K. K. Lee and P. A. Lee, Physica B **259-261**, 481 (1999).

[42] This dressed energy is the sum of the dressed energy of spinon and that of antiholon near the equilibrium Fermi surface.

[43] N. Andrei, Phys. Lett. A **87**, 299 (1982).

[44] A. O. Gogolin, R. M. Konik, A. W. W. Ludwig, and H. Saleur, Ann. Phys. (Leipzig) **16**, 678 (2007).

[45] The equality can be proved analytically in linear response. In numerics we also see very good agreement, especially for large voltage, with voltage computed by $\mu_1 - \mu_2$ given by free energy and voltage computed by difference in particle number.

[46] F. D. M. Haldane, Phys. Rev. Lett. **40**, 416 (1978).

[47] E. Lebanon and A. Schiller, Phys. Rev. B **65**, 035308 (2001).

[48] A. C. Hewson, A. Oguri, and D. Meyer, Eur. Phys. J. B **40**, 177 (2004).

[49] J. Paaske and K. Flensberg, Phys. Rev. Lett. **94**, 176801 (2005).

[50] A. C. Hewson, *The Kondo Problem to Heavy Fermions* (Cambridge University Press, Cambridge, 1993).

[51] Here we adopted the Kondo scale as in the article by N. S. Wingreen and Y. Meir, Phys. Rev. B **49**, 11040 (1994). We use a factor of $\sqrt{10}$ to increase this scale so the Kondo peak can be observed more easily in numerics.